An Antireflective Top Contact for Optoelectric Devices Using Niobium Doped Titanium Dioxide

A thesis submitted by

John E. Chivers

In partial fulfillment of the requirements for the degree of

Master of Science in Electrical Engineering

TUFTS UNIVERSITY

May, 2012

ADVISER: Thomas E. Vandervelde, PhD.

Abstract

This work outlines an effort to design and optimize a complete top contact system for use with photovoltaic cells. The system will incorporate a transparent conductor and a two-stage antireflective treatment. To create an economically sustainable design, choice of materials is restricted to those that do not require large amounts of rare-earth elements – specifically indium, which is the main ingredient in the current industry-standard transparent conductor, indium-tin-oxide. The proposed system will use niobium-doped titanium dioxide (TNO) as the conductor combined with a continuously graded antireflective coating composed of titanium dioxide and silicon dioxide. To further suppress reflection of incident light, the silicon dioxide surface will be etched to form a nano-scale "moth's eye" pattern. This report details the first stage of the research project which focuses on material characterization and conductor fabrication.

Acknowledgments

My advisor, Prof. Thomas Vandervelde, patiently provided guidance, advice and encouragement. Thanks Tom.

My thanks to Prof. Jeffery Hopwood for generously sharing his time and his expertise.

Critical funding for the reconstruction of an ion beam deposition system was provided by The Peter and Denise Wittich Family Fund.

The experimental portion of this work would not have been possible without the tools provided at the Center for Nanoscale Systems and at Tufts Micro & Nano Fabrication Facility. The expertise of the faculty and staff at both facilities was invaluable.

Table of Contents

Chapter 1 - Introduction 2

Proposal 2

Chapter 2 – Background 9

TCOs 9

Transparency 12

Conductivity 15

Ohmic Contacts 18

Antireflective Coatings 21

Chapter 3 – Materials and Methods 27

Magnetron Sputter 27

Ion Beam Sputter 29

E-Beam Evaporator 30

Rapid Thermal Processor 32

Tube Furnace 32

Profilometer 33

Ellipsometer 34

Hall Effect System 39

Chapter 4 – Rebuild of Ion Beam Sputter Tool 42

Initial Condition 42

Rebuild 44

Low Beam Current 48

Secondary Ion Beam 52

DC Magnetron 52

Current Status 53

Chapter 5 – Results 54

TCO Optical Properties 55

TCO Electrical Properties 58

Chapter 6 – Future Work 60

Moth's Eye 60

Fabrication 62

Appendix 1 SOP for Ion Beam Deposition System 64

Appendix 2 Drawings of Substrate Holder for Ion Beam Deposition System 72

List of Figures

Figure 1-1: Proposed top contact system: a conductive layer of niobium-doped titanium dioxide, a continuously graded anti-reflective layer of titanium dioxide and silicon dioxide, and an antireflective nanostructured surface 2
Figure 1-2: SEM (left) and AFM (right) images of moth's eye pattern etched on ALON [8] 7
Figure 2-1: The complex index of refraction for indium tin oxide; the plasma frequency occurs at approximately 1425nm, where the extinction coefficient becomes larger than the real index. 15
Figure 2-2: Conduction electrons: (a) in a metal, conductions electrons are always present; (b) in a semiconductor, a small amount of energy is needed to promote an electron to the conduction band; (c) in an insulator, a large amount of energy is needed to promote an electron to the conduction band. 16
Figure 2-3 When a metal is brought into contact with a semiconductor, charge will redistribute across the interface until the Fermi levels are equalized. This results in a potential gradient across the interface region. [6] 19
Figure 2-4 Schottky contacts on n-type semiconductor: Left, metal with large work function forces down the Fermi level of the semiconductor, current will flow easily into the semiconductor; Right, metal with small work function forces up the Fermi level of the semiconductor, current will flow easily out of the semiconductor[6]. 20
Figure 2-5: Reflection and transmission at a material interface 22
Figure 3-1: The 6-target sputtering system at CNS and a magnetron sputtering gun [2, 7] 27
Figure 3-2: Magnetron sputtering: ions from a magnetically confined plasma are driven into a target and dislodge material from the target [4]. 28
Figure 3-3: Ion beam sputtering; material is removed from the target by a stream of high velocity ions [3]. 29
Figure 3-4 One of the electron beam evaporators at CNS [2]. 31
Figure 3-5: Dektak profilometer at TMNF 34

Figure 3-6: By reflecting light off a surface and measuring the change in polarization, an ellipsometer is able to determine the thickness and optical constants of a material. 35
Figure 3-7: Measured values of psi (green) and the best fit generated by modeling software (red) for a sample of semiconductor; the fit is quite good except at the lowest wavelengths where the material is approaching its band gap. 38
Figure 3-8 Hall effect measurement system and the sample chamber [1] 39
Figure 3-9: The Hall Effect: a carrier with charge q and velocity v is deflected by a force F induced by the applied magnetic field B causing charge build up which produces the Hall voltage V_H [5]. 40
Figure 4-1: Ion beam deposition system. 42
Figure 4-2: Chamber of ion beam tool. 47
Figure 4-3: Plasma source base and cathode before cleaning. 49
Figure 4-4: Plasma source base and anode before cleaning. 49
Figure 5-1: Model of optical behavior of TNO sample. Experimental values of Δ (green) and the best fit model (red). 56
Figure 5-2: Model of optical behavior of TNO sample. Experimental values of ψ (green) and the best fit model (red). 56
Figure 5-3: The real index of refraction for a TNO sample. 57
Figure 6-1: The surface of a moth's eye; a coating of sub-wavelength cones reduces reflection of visible light helping the moth to evade detection by predators[Newscom]. 61

An Antireflective Top Contact for Optoelectric Devices Using Niobium Doped Titanium Dioxide

Chapter 1 - Introduction

Proposal

This work outlines an effort to design and optimize a complete top contact system for use with photovoltaic cells. The system will incorporate a transparent conductor and a two-stage anti-reflective treatment. To create an economically sustainable design, choice of materials is restricted to those that do not require large amounts of rare-earth elements – specifically indium, which is the main ingredient in the current industry-standard transparent conductor, indium-tin-oxide. The proposed system (Figure 1-1) will use niobium-doped titanium dioxide (TNO) as the conductor combined with a continuously graded anti-reflective coating composed of titanium dioxide and silicon dioxide. To further suppress reflection of incident light, the silicon dioxide surface will be etched to form a nano-scale "moth's eye" pattern.

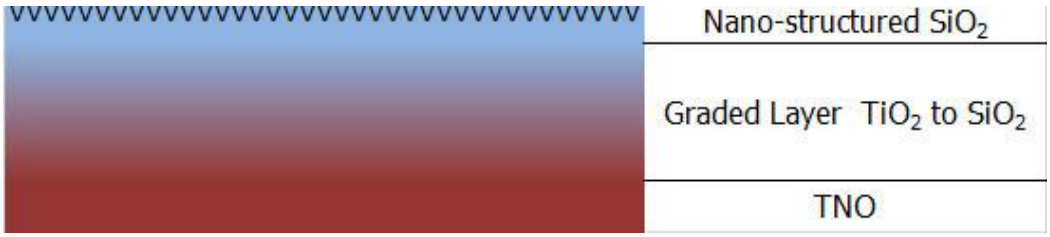

Figure 1-1: Proposed top contact system: a conductive layer of niobium-doped titanium dioxide, a continuously graded anti-reflective layer of titanium dioxide and silicon dioxide, and an antireflective nanostructured surface

The current industry standard transparent conducting oxide (TCO) is tin-doped indium oxide (ITO)[8], but the increasing scarcity and, therefore, expense of indium is driving a search for alternative materials[9, 10]. Indium is currently being refined at a rate of approximately 600 tons per year (568 tons in 2008)[11]. Most of this indium is used in the form of ITO by flat panel display manufacturers[12]. The demand for indium is increasing as the demand for flat panels increases, but the worldwide commercially viable reserve is estimated to be only 5600 tons (according to the U.S. Geological Survey in 2010)[13]. It is clear that demand will soon exceed supply.

Motivated by the approaching indium shortage, many researchers have been investigating indium-free TCOs[14]. Many materials have been studied, and several promising candidates have emerged. Excellent results have been achieved with compounds of zinc oxide. Gallium doped zinc oxide (GZO) has demonstrated electrical and optical behavior comparable to ITO[15]. Gallium itself is just as scarce as indium, but GZO contains only 2% to 3% gallium oxide whereas ITO is 80% to 90% indium oxide[14]. In ITO, indium oxide is the bulk material; in GZO, gallium oxide is the dopant. Aluminum-doped zinc oxide (AZO) also shows promise; its conductivity is inferior to ITO or GZO, but it contains no rare or toxic constituents. AZO could be an excellent material for less demanding applications[16].

Another promising candidate is niobium-doped titanium oxide (TNO). TNO has shown performance comparable to (if not yet equaling) ITO, and there is

ongoing research to improve performance[17]. As with indium and gallium, niobium is a scarce resource but, like the gallium in GZO, TNO contains only a relatively small (<5%) amount of niobium oxide. TNO has properties which could make it especially desirable for certain applications: a low plasma frequency (plasma wavelength > 3μm) which makes it useful for infrared devices, a very high index of refraction (n>2.4 in the visible) which can provide better optical coupling to high index semiconductors, and excellent chemical stability and physical durability[17].

ITO, however, is still superior to TNO in one important aspect: processing temperature. ITO can be deposited and annealed without exceeding a temperature of 150°C[9]. TNO, according to current publications, requires a processing temperature of 450°C to achieve peak performance[17]. For some applications this high temperature is not an issue; for other applications this makes TNO completely unsuitable. Fortunately, many devices are built "top down", with the TCO deposited first and then followed by the other device layers. For this type of fabrication the TNO processing temperature should not be a concern.

As mentioned, transparent conductors play a critical role in the design of photovoltaic cells. The ability of a TCO to make electrical contact with the entire surface of a PV cell without blocking incident light offers a marked improvement in device efficiency over earlier techniques. Previously, top contacts were formed by depositing a metal grid on the surface which blocked a significant percentage

of incident light and provided poor electrical extraction due the fact that it was in contact with only a small portion of the surface[18]. Both of these effects reduced device efficiency. The development of ITO, an effective and affordable transparent conductor, was an important step forward in the progress of PV technology. The development and optimization of high-performance, indium-free, alternatives is critical to the future of the PV industry.

For this work, TNO was chosen as the conductor for the proposed top contact system for several reasons: First, it displays electrical and optical performance on par with ITO or GZO. Second, it uses only a small amount of rare earth material and, while the use of any rare earth material is not ideal, the superior performance afforded by the incorporation of the niobium dopant is needed for high performance PV applications. Third, the exceptionally large window of transparency, extending well into the infrared, makes TNO ideal for use with wide-spectrum, multi-junction solar cells (or thermophotovoltaic cells operating in the near IR). Lastly, the crystalline structure of titanium dioxide shows excellent compatibility with silicon dioxide, allowing the two materials to be easily blended into a stress-free crystalline composite[19]. This compatibility with silicon dioxide will be exploited to form an anti-reflective layer on top of the conductive layer.

To further improve efficiency in PV devices, anti-reflective coatings (ARCs) are normally applied to the top contact. Traditional ARCs use multiple layers of materials with decreasing indices of refraction to make the index change in

several steps. Making the transition in several small steps, instead of one big one, produces less reflection because reflectivity is proportional to the square of the differences of the indices of the two materials. Performance is improved by using more layers, making the transition in smaller steps. When taken to the logical limit, this results in a continuously graded film which, in theory, produces no reflection. The proposed design incorporates this type of continuously graded ARC. The similarities in the crystalline structures of TiO_2 and SiO_2 should make it possible to reliably fabricate a continuously graded film to transition from the TNO conductor (n=2.3) to pure glass (n=1.4).

ARC techniques employing a quarter-wave interference effect are not considered due to their poor performance outside of a narrow frequency band.

The proposed graded ARC terminates with a pure SiO_2 surface which will reflect light at the air/SiO_2 interface. Using traditional ARC techniques, there is little that can be done to mitigate this reflection. To move beyond the limits of conventional anti-reflective coatings, it will be necessary to design and fabricate a nanostructured surface. Patterning a film surface with structures of the same size scale as the incident light wavelength allows for manipulations of a material's optical behavior that are not otherwise possible[20]. The strategy of using bulk material properties in combination with nanostructure surface effects offers an improved level of control over optical properties. Nano-scale manipulation of material properties has expanded the technological possibilities in many fields of science, engineering, and manufacturing. The amount of

research being conducted in this field has grown dramatically in recent years and technologies developed are already in use in industry.

The proposed system will have a "moth's eye" pattern etched into the SiO_2 surface (Figure 1-2). A regular pattern of sub-wavelength scale (<300nm) cones rising from the glass surface will create a gradual optical transition between air

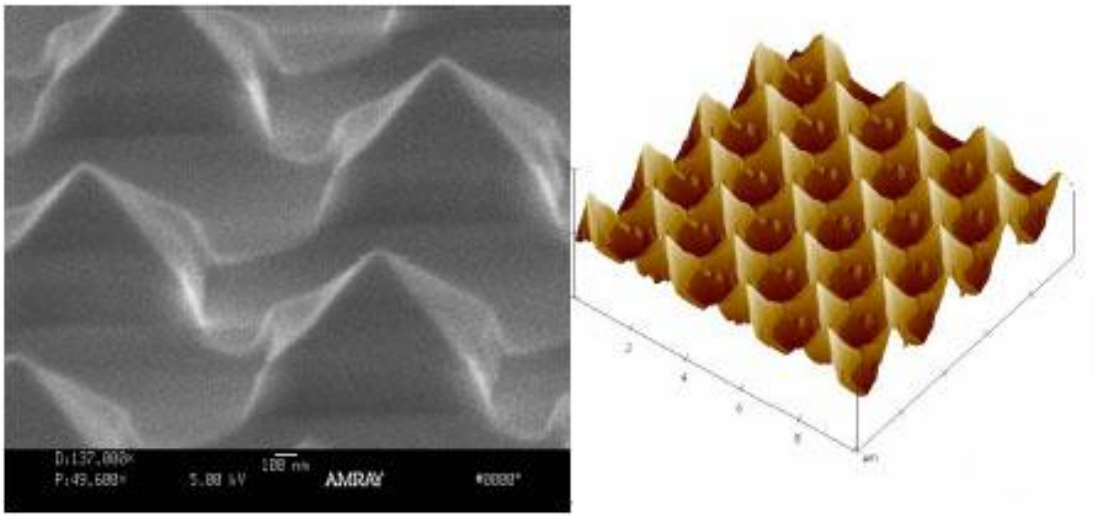

Figure 1-2: SEM (left) and AFM (right) images of moth's eye pattern etched on ALON [8]

and glass. In theory, this would suppress all reflection at all wavelengths longer than the feature size of the etched pattern[21].

Deposition of the TNO and graded ARC layers can be done with standard RF magnetron sputtering. The moth's eye pattern can be created by forming a template with electron-beam lithography (or, possibly, with self-assembling

nano-particles) followed by a wet etch in hydrofluoric acid or a dry etch in a reactive ion etcher.

The technologies that deliver light into, and extract current from, photovoltaic devices can be as important as those that generate the charge carriers, and advancement in these areas is critical to improving the performance of power generation and photo-detection systems. The integrated top contact system proposed here could provide a high conductivity, high transparency contact using abundant, well characterized materials that can be integrated into an existing product line quickly and cheaply.

Chapter 2 – Background

TCOs

Transparent conducting oxides (TCOs) are, as the name suggests, materials that are both optically transparent and electrically conductive. They are used extensively in optoelectric devices (photovoltaic cells, photo detectors, light emitting devices) as the "top contact" which must be able to extract current without blocking the incident light[14]. These materials are also used extensively in the production of flat panel displays and other devices that require transparent electrical connections[22]. This work will focus on the use of TCOs as the top contact for inorganic photovoltaic devices.

The first observed TCO was an oxidized cadmium film reported by Badeker in 1907[23]. This initial discovery sparked some academic interest, but development of transparent conductors was slow through the first half of the twentieth century. This can be explained by the lack of industrial applications at that time and by the well documented and exceptional toxicity of cadmium. Few people are eager to work with a highly toxic material that has few practical applications.

Conductivity in a blend of indium-oxide and tin-oxide was first reported in 1947[9] and by the 1960s an ITO deposition method was available for commercial applications[9]. ITO can be deposited using sputtering or spray on

techniques followed by annealing (or, alternatively, in-situ annealing with a heated substrate). When deposited correctly, ITO typically has a resistivity of about $1x10^{-4}$ Ωcm[24]. A variety of other materials have been tested as transparent conductors including, but not limited to, oxides of cadmium, tin, and zinc compounded with various dopants. None were able to match the performance of ITO.

In the first years of the 21st century, with the commercialization of flat panel technology and the increased desire for solar power, the demand for ITO rose dramatically. It became apparent that the demand for indium would soon exceed the available supply. According to figures published by the U.S. Geological survey in 2010, the world's known indium reserves will be exhausted around the year 2020[13]. Clearly, a high performance, indium-free TCO is needed.

Efforts in the U.S., and at the National Renewable Energy Laboratory in particular, have focused on zinc-oxide [14, 25]. Two formulations have demonstrated excellent results. Zinc-oxide doped with gallium-oxide (GZO) demonstrates performance comparable to, if not quite equaling, ITO. Gallium is itself a somewhat scarce resource, but GZO is formulated with less than 5% gallium-oxide. ITO is about 90% indium-oxide. GZO should be a commercially viable alternative to ITO. Zinc-oxide doped with aluminum-oxide (AZO) shows poorer conductivity but uses no rare elements and could be an excellent alternative for applications that do not require high conductivity.

Several other research groups (particularly at Kanagawa Academy of Science and Technology, Tohoku University, and The University of Tokyo) have been investigating titanium oxides doped with niobium-oxide (TNO)[26]. The optical transmission and electrical conductivity are on par with GZO and niobium is about as scarce as gallium. This would make TNO and GZO equally attractive as ITO alternatives. However, TNO also has some qualities that could make it more attractive for certain applications. TNO has a wide window of transparency, extending through the visible and into the infrared to about 3 microns, which makes it appealing for broad spectrum devices such as multi-junction solar cells. The high index of refraction is also appealing for semiconductor applications.

In recent years, a great deal of research has been conducted to investigate the basic physics behind the behavior of TCOs, including: band structures of competing oxide formulations [27, 28], temperature dependence[27], conduction pathways[28], carrier mobility[28, 29], carrier concentration[30], Ohmic contact formation[31, 32], optical absorption[33, 34], thermal stability[35], and deposition techniques[15, 17, 28, 36-38].

Over the past decade, The Materials Research Society has shown a keen interest in the development of TCOs[8, 22, 30, 39, 40]. In 2007 the MRS Bulletin published a review of the current state of research for TCOs for photovoltaic applications; this paper emphasized the importance of research on novel TCOs that do not rely on Indium or other exotic components[14].

Transparency

Light will pass through a material unless some mechanism within the material prevents transmission. There are a number of ways that incident light can be absorbed or reflected and, in any given material, different mechanisms can operate at various frequency ranges. The TCO materials used in this research were chosen for their high level of transmission in the visible and near infrared regions of the electromagnetic spectrum. Typically, in semiconductor materials, incident light of higher frequency is absorbed through a band gap excitation and light of lower frequency is absorbed through excitation of free electrons[14, 22].

Band gap refers to the energy required to move an electron from the valence band to the conduction band, that is, to move it from a state where it is tightly bound to one atom in a crystal lattice to a state where it is only loosely bound and can therefore move relatively freely through the crystal. If an incident photon has energy equal to or greater than the bang gap energy, then the photon will be absorbed by a valence electron. If the photon has an energy lower than the band gap, then it cannot be absorbed by a valence electron and will continue through the material unimpeded. The band gap for semiconductors is quite low, which is what makes them semiconductors; it is very easy to promote electrons to the conduction band, and thus, increase the electrical conductivity of the material. Materials chosen for use as TCOs must have a band gap large enough to prevent absorption of photons in the desired region of transparency. If, as is usually the case, transmission of visible light is desired,

then the band gap should be in the ultraviolet region. However, since conductivity is also required, it is desirable to have a band gap as low as possible without impairing visibility, the lower band gap allowing more electrons to be promoted to the conduction band. To provide the best optical and electrical behavior, materials are chosen which have a band gap very near the edge of the visible spectrum[14, 41].

Metals are characterized by an abundance of free electrons, electrons that permanently occupy the conduction band. TCOs have free electrons provided by their dopants and, although TCOs don't have nearly as many free electrons as metals, they do have enough to provide adequate electrical conduction. Free electrons can absorb photons, however, which limits the transparency of the material. Since these electrons are able to oscillate freely within the crystal, they can absorb photons of any energy, up to a point. Free electrons are not entirely free; as they oscillate they do experience a restoring force from the fixed positive charges in the crystal lattice. At higher frequencies this restoring force makes it difficult for the free electrons to respond to the driving force of the photon; the electron can't move fast enough to keep up with the photon. Above a certain point, known as the plasma frequency, the free electrons are unable to interact with these higher energy photons and no absorption occurs. Most metals have a plasma frequency in the ultraviolet region (gold and copper are in the visible region which is what gives them their unusual coloring). For a TCO to maintain transparency, its plasma frequency must be low enough to prevent free electron absorption in the desired region of transparency. The choice of dopant and the

doping concentration play a major role in determining the plasma frequency[42, 43].

Plasma frequency can be calculated, if other material properties are known, as follows:

$$\omega_p = \sqrt{\frac{ne^2}{\varepsilon_0 \varepsilon_\infty m^*}}$$

Where n is the carrier concentration, e is the carrier charge, ε_∞ is the material's permittivity at infinite frequency, ε_0 is the permittivity of free space, and m* is the effective mass of the carrier[9]. Normally, it is much easier to determine the plasma frequency experimentally and then use that to determine the values of other, more difficult to measure, properties, such as the effective mass. Plasma frequency can be determined simply by inspection of a plot of the complex index of refraction as a function of wavelength, if one is available. It is, by some

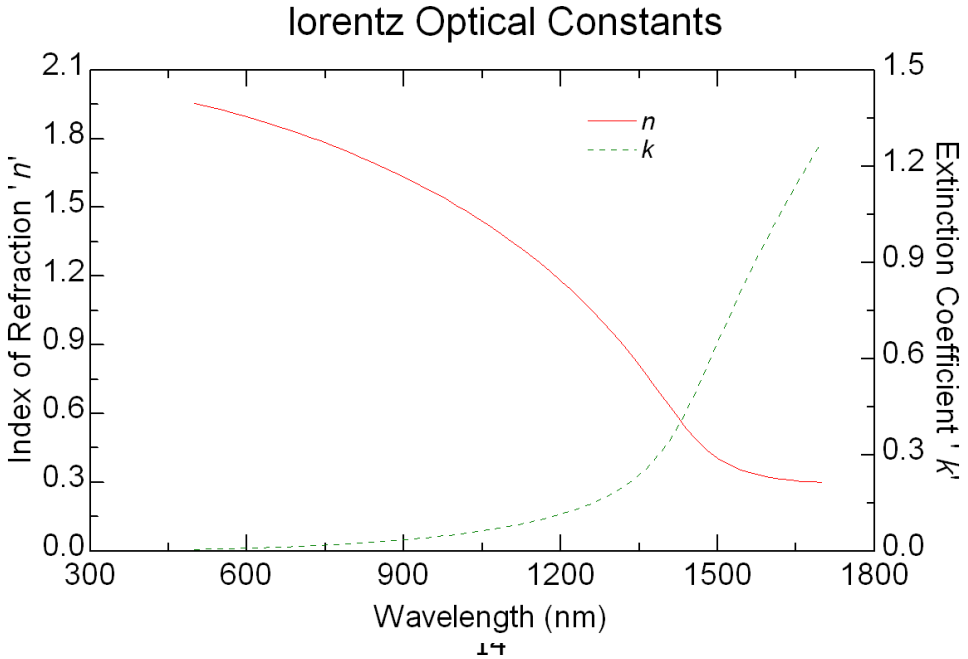

definitions, the point at which the imaginary component of the index becomes greater than the real component (Figure 2-1)[42]. Similarly, band gap can be predicted with modeling software, but it is normally more practical to determine it experimentally.

Conductivity

When an electric field is applied across a material, charge carriers will move through the material in response to the field if there are carriers present. In most applications, including this work, the relevant charge carrier is the electron. Materials that feature negatively charged carriers, such as electrons, are called n-type. All the TCOs discussed in this work are n-type. Materials that use positively charged carriers are called p-type. P-type TCOs have been reported, but the performance of these new materials is not yet adequate for practical

Figure 2-1: The complex index of refraction for indium tin oxide; the plasma frequency occurs at approximately 1425nm, where the extinction coefficient becomes larger than the real index.

applications.

In metals (Figure 2-2a), many free electrons are available to act as charge carriers. Free electrons are electrons that are bound to the material but not bound to any particular location in the crystalline lattice formed by the metal atoms. In the absence of an applied field, they distribute themselves in a manner appropriate to maintain electrostatic equilibrium. In response to an applied field, they will move quite freely in comparison to the carriers in most other conductive

materials and loose very little energy to internal interactions (low resistance). This abundance of free electrons also makes metals opaque to visible light; free electrons will readily absorb photons in the visible range.

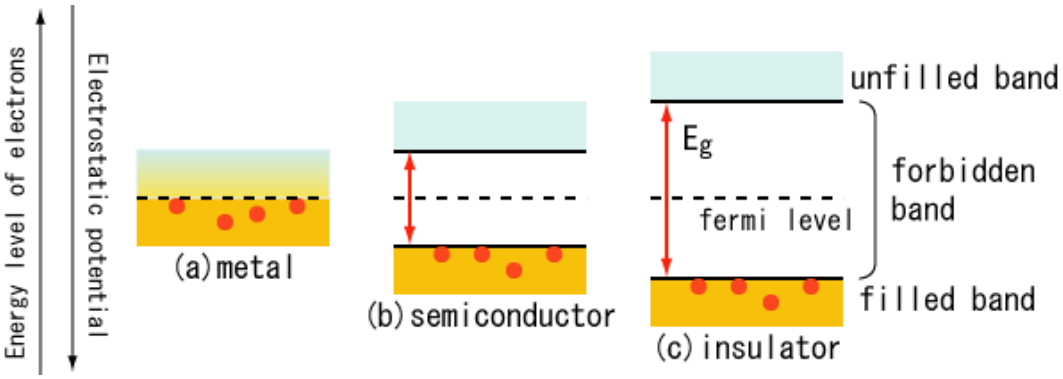

Figure 2-2: Conduction electrons: (a) in a metal, conductions electrons are always present; (b) in a semiconductor, a small amount of energy is needed to promote an electron to the conduction band; (c) in an insulator, a large amount of energy is needed to promote an electron to the conduction band.

In semiconductors (Figure 2-2b), electrons will only be available to act as conductors if they are given enough energy to separate them from a localized potential well in the atomic lattice of the material. Once freed, the electron will, for a short time, act very much like the free electrons in a metal. The energy required to promote an electron to a conductive state is called the band gap. Incident photons without the energy required to promote an electron across the band gap will not be absorbed by this mechanism. This behavior is integral to the function of photovoltaic devices and the semiconductors in PV devices are normally chosen to have a band gap accessible to visible light. For this reason,

PV semiconductors are opaque to visible light. Semiconductors used for transistor fabrication are chosen to have a band gap small enough to allow easy electron promotion when desired but large enough to prevent promotion due to thermal excitation. These materials are also typically opaque to visible light.

Insulators (Figure 2-2c) can be viewed simply as semiconductors that have very large band gaps; band gaps large enough to effectively prevent any electron promotion. This inability to absorb photons in a band gap transition is what makes many insulators transparent to visible light. In fact, nearly any material transparent to visible light, glass as the most common example, can be expected to be an excellent insulator.

The conduction mechanisms in TCOs are, at this time, not well understood. It seems clear that the dopant materials in n-type TCOs are supplying the materials with free electrons. Successful dopant choices have always been atoms with one more valence electrons than the bulk material so that when the dopant is incorporated in the bulk lattice it will have one electron left unattached to the lattice and, therefore, much more able to free itself from the lattice. The choice of a dopant that is heavier than the bulk material has also been beneficial; the valence electrons of larger atoms are more loosely bound to the nucleus, and so, are easier to remove. Another key factor in TCO conductivity seems to be the presence of oxygen vacancies in the crystal structure of the oxide. Perfectly stoichiometric oxides display little or no conductivity. It is believed that the vacancies give the free electrons a lower-resistance path through the material.

This interaction with oxygen vacancies is not well understood and is a current focus of research in the field.

As can be seen from this discussion, conductivity and transparency are inherently interrelated and, in most materials, mutually exclusive. This conflict has made it quite difficult to produce viable transparent conductors and in all cases compromises in material properties have been required. All TCOs absorb more light than pure insulators like glass and no TCO has demonstrated conductivity that can compare to a metal. For some applications, these limitations are acceptable as neither ideal transparency nor ideal conductivity is required. Photovoltaic devices, however, are not so forgiving. Photons that are lost to absorption in the top contact and output current lost to poor electrical conduction will both reduce the overall device efficiency. It is this need for maximum performance in PV applications that has, in large part, been the driving motivation behind the development of transparent conductors.

Ohmic Contacts

Metal contact pads must be applied to a TCO surface as connection points for the wiring used to connect the device to any external system. Metal to semiconductor junctions have been in use throughout the history of the semiconductor industry, but their design and fabrication can still present significant difficulties. The challenge is to create a junction that does not have an inherent bias that will oppose the flow of current.

When a metal and a semiconductor are brought into contact, the Fermi levels of the two materials will align, causing band bending in the energy structure of the semiconductor near the interface (Figure 2-3). This band bending is due to charge carriers moving across the interface. An equilibrium state is reached when enough charge has crossed the interface to equalize the Fermi levels. This

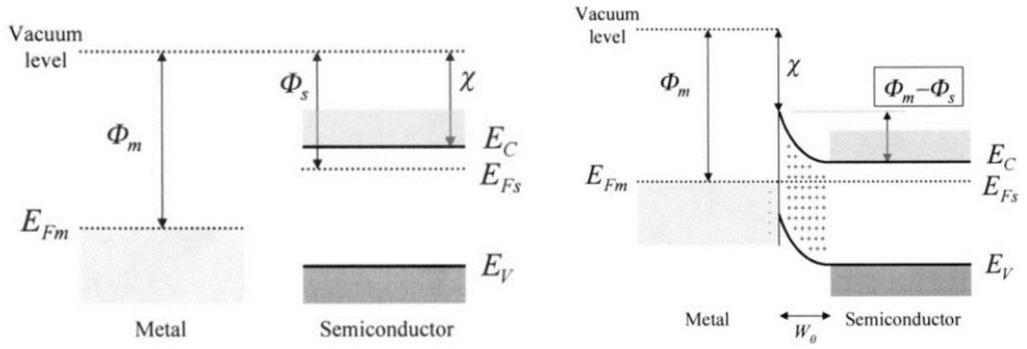

Figure 2-3 When a metal is brought into contact with a semiconductor, charge will redistribute across the interface until the Fermi levels are equalized. This results in a potential gradient across the interface region. [6]

redistribution of charge creates a potential difference between the two materials which can impede current flow if the potential barrier is in opposition the current [41, 44].

When the Fermi levels of two materials are very nearly equal, then only a very small potential barrier forms and current will flow in either direction with very little impediment; this is known as an Ohmic contact. Fabrication of Ohmic contacts can be difficult as the fabricator must know the Fermi level of the semiconductor and then choose a contact metal with a very similar level. Determining the Fermi level of any semiconductor is a challenge; doping levels,

impurities, and crystal defects will all alter the position of the Fermi level. Even if the semiconductor is well characterized, there may not be a metal available that meets the need; metals generally have a higher work function (the difference between the Fermi level and the vacuum level, Φ) than semiconductors. Adding to these difficulties, surface defects, oxidation, and material contamination will alter the material properties at the interface. Fabrication of truly, or nearly, Ohmic contacts can be a great challenge.

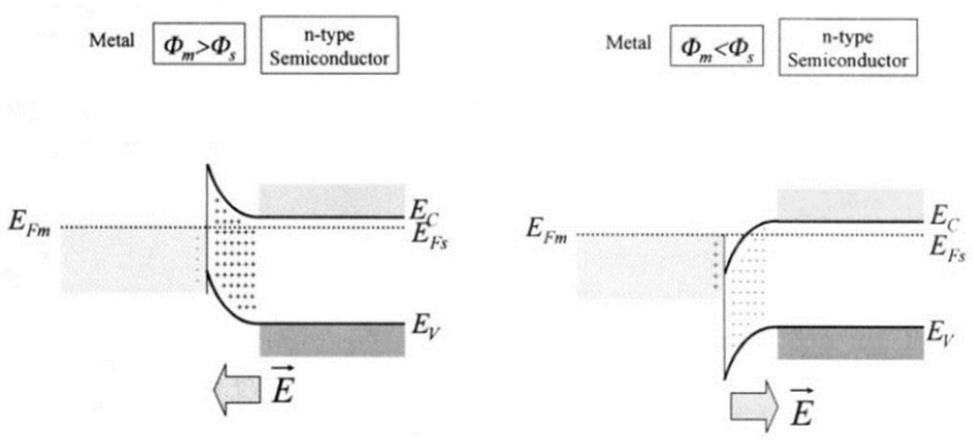

Figure 2-4 Schottky contacts on n-type semiconductor: Left, metal with large work function forces down the Fermi level of the semiconductor, current will flow easily into the semiconductor; Right, metal with small work function forces up the Fermi level of the semiconductor, current will flow easily out of the semiconductor[6].

Good electrical contacts can be made with much less difficulty if current flow is only required in one direction. The potential barrier formed only impedes current flow in one direction, so contacts can be made that allow free current flow in a

chosen direction. This type of contact is called a rectifying contact or a Schottky contact. The direction and size of the barrier depends on the work functions of the two materials and the carrier type in the semiconductor. Figure 2-4 illustrates two rectifying contacts formed on an n-type semiconductor; one in which the metal has a higher work function than the semiconductor and on where the metal has a lower work function[6, 41, 45].

The same principles hold for p-type semiconductors and Schottky contacts can be fabricated for either direction of current. No p-type materials were used in this research.

In a commercially distributed device, Schottky contacts are often sufficient as bidirectional current is not required. Unfortunately, in a research and development setting, bidirectional current flow is often required for the testing procedures used to characterize new materials. Hall Effect measurements, as an example, are extremely useful for understanding the electrical properties of semiconductors but they are dependent on contact quality.

Antireflective Coatings

At the interface between materials of differing indices of refraction, some of the light incident on the interface will transmit through to the second material and some will be reflected back into the first material (Figure 2-5). For an ideal, flat

surface, the transmission and reflection angles are dependent on the incident angle and the indices of refraction according to:

$$Transmission: \ n_i \sin\theta_i = n_t \sin\theta_t$$

$$Reflection: \ \theta_r = -\theta_i$$

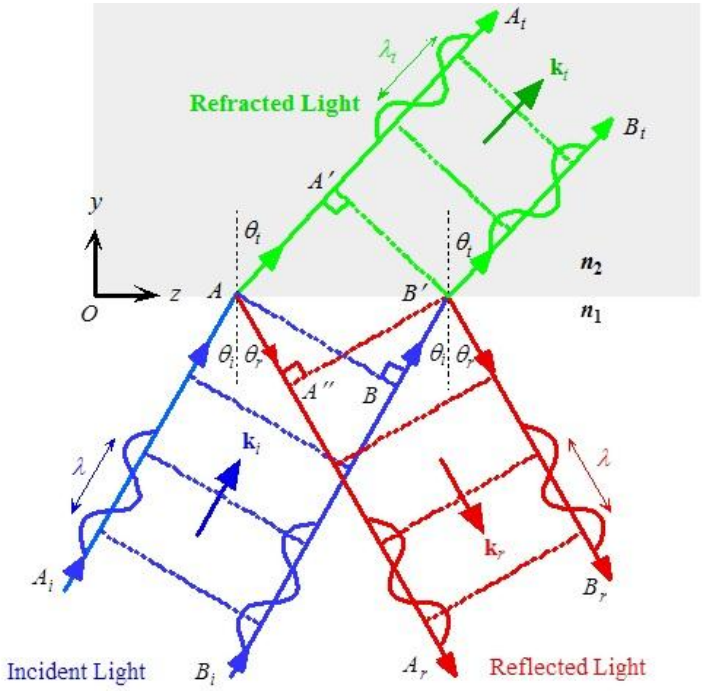

Figure 2-5: Reflection and transmission at a material interface

The magnitudes of reflection (as a fraction of incident magnitude) can be calculated for the simplest ideal case of light incident on a flat surface at normal angle for homogeneous, non-magnetic, non-absorbing materials as:

$$R = \left(\frac{n_2 - n_1}{n_2 + n_1}\right)^2$$

$$T = \frac{4n_2 n_1}{(n_2 + n_1)^2}$$

To allow for light incident at angles other than the normal, slightly more involved calculations are required. For non-absorbing materials:

$$R_\perp = r_\perp^2$$

$$R_\parallel = r_\parallel^2$$

$$T_\perp = \left(\frac{n_2 \cos\theta_2}{n_1 \cos\theta_1}\right) t_\perp^2$$

$$T_\parallel = \left(\frac{n_2 \cos\theta_2}{n_1 \cos\theta_1}\right) t_\parallel^2$$

Where r and t are the reflection and transmission coefficients expressed as the perpendicular and parallel polarization components defined for non-magnetic, non-absorbing, homogeneous materials as:

$$r_{\perp} = \frac{n_1 \cos\theta_1 - n_2 \cos\theta_2}{n_1 \cos\theta_1 + n_2 \cos\theta_2}$$

$$r_{\parallel} = \frac{n_2 \cos\theta_1 - n_1 \cos\theta_2}{n_1 \cos\theta_2 + n_2 \cos\theta_1}$$

$$t_{\perp} = \frac{2\, n_1 \cos\theta_1}{n_1 \cos\theta_1 + n_2 \cos\theta_2}$$

$$t_{\parallel} = \frac{2\, n_1 \cos\theta_1}{n_1 \cos\theta_2 + n_2 \cos\theta_1}$$

Removing one restriction from ideality adds a great deal of complexity to the calculations. Removing the restrictions regarding non-magnetic, non-absorbing, homogeneous materials, and keeping in mind that the equations above are for a single wavelength of incident light (the index of refraction is wavelength

dependent), would result in exceptionally difficult calculations. For this reason, all attempts to model optical behavior were conducted using commercially produced software.

Simple models, however, should be sufficient to understand the behavior of antireflective coatings. The device proposed here incorporates two types of antireflective treatments: a continuously graded coating and nano-structured surface.

The most commonly used antireflective coating (ARC) is the quarter-wave technique which uses a film with a thickness one quarter that of the wavelength of the incident light to generate interference that cancels reflected light. This method works quite well at a single wavelength. Usually this technique is used for applications involving human sight (e.g. sunglasses) and a yellow-green wavelength is chosen to suit the sensitivity of the human eye. Quarter-wave techniques were not considered for the proposed device as it requires high transmission across a wide spectrum (300nm to 3000nm). To accommodate a broad spectrum of incident light it is necessary to use techniques that do not directly depend on the wavelength of the light.

The first technique considered is a continuously graded coating. To transition between two materials with different indices of refraction (e.g. TiO_2 and SiO_2) with minimal reflection it is best to make the transition in several (or many) small steps as opposed to one large step. Since the magnitude of reflection at an interface is proportional to the square of the difference of the indices of

refraction, total reflection can be reduced by dividing the total change in index into multiple smaller changes. If the total change in index could be accomplished in an infinite number of infinitesimal steps then the reflection would be reduced to nothing. Something like this can be accomplished if the two materials can be blended at the interface to form a continuously graded transition between materials with an accompanying continuous change in the index of refraction.

Busani and Devine have investigated the electrical and optical properties of various forms of TiO_2 and TiO_2/SiO_2 mixtures[46, 47]. In a mixed film, they were able to vary the refractive index from 1.46 to 2.3 by adjusting the Ti concentration[19]. This research supports the viability of the TiO_2/SiO_2 mixture.

The second technique is a nano-structured pattern applied to the surface of the device to reduce reflection at the air/SiO_2 interface. This is the moth's eye effect which will be discussed in greater detail in the chapter on future work.

Chapter 3 – Materials and Methods

This research required the use of a variety of tools. They were needed to deposit TCO films onto substrates, to deposit metal contacts onto the TCO films, and to measure the optical and electrical properties of the materials.

Magnetron Sputter

Deposition of TCO and other dielectric materials was done using the 6-target sputtering system (manufactured by AJA International) at the Center for Nanoscale Systems (CNS) at Harvard University (Figure 3-1).

Figure 3-1: The 6-target sputtering system at CNS and a magnetron sputtering gun [2, 7]

Magnetron sputter systems (Figure 3-2) generate a plasma in a vacuum chamber and use an applied voltage to accelerate the ions from the plasma. The plasma is

magnetically confined near a target and the applied voltage drives ions into that target. These ion impacts eject material from the target which then deposits on other surfaces in the chamber including the substrate. The plasma is formed in front of the target and the source of the accelerating bias is positioned behind the target; with this arrangement, a simple DC bias can be used with conductive targets, but non-conducting targets require an RF bias[48-50]. The six target system at CNS is equipped with three DC magnetrons and three RF magnetrons; the RF guns were used for all TCO and SiO_2 depositions.

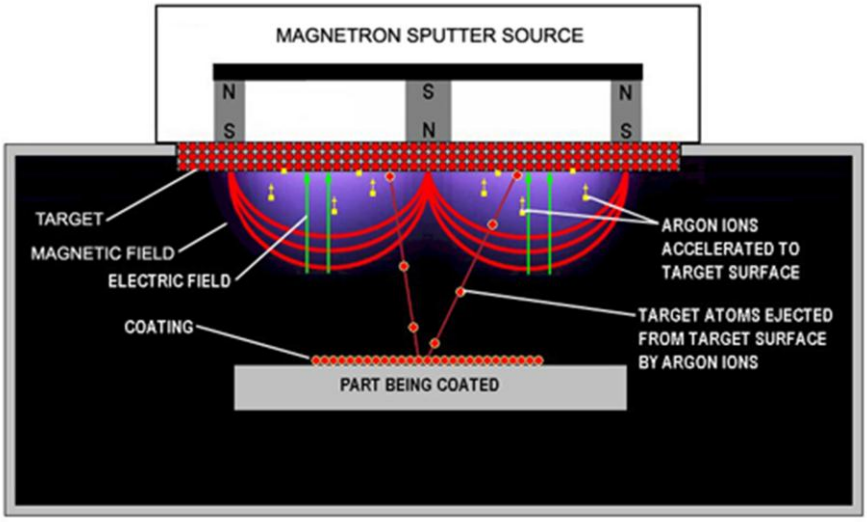

Figure 3-2: Magnetron sputtering: ions from a magnetically confined plasma are driven into a target and dislodge material from the target [4].

The six target system was chosen simply because it was the only tool available that was capable of depositing TCO materials. Fortunately, this tool has capabilities which make it ideal for the deposition of optical films. The pumping system uses a cryo-pump and a load-lock which allows the chamber to reach a

base pressure on the order of 10^{-8} Torr almost instantly after loading a new substrate. This high vacuum environment is critical for the production of high purity films. The tool can bias the substrate holder to perform an in-situ plasma clean of the substrate to remove organic contaminants. It can also alter the deposition conditions with a substrate heater and oxygen or nitrogen gas flow in the deposition chamber; these latter capabilities were not used on this project but could prove useful for optimizing the performance of TCO materials.

Deposition of some metal contacts was done with the DC sputtering system at the Tufts Micro & Nano Fabrication Facility.

Ion Beam Sputter

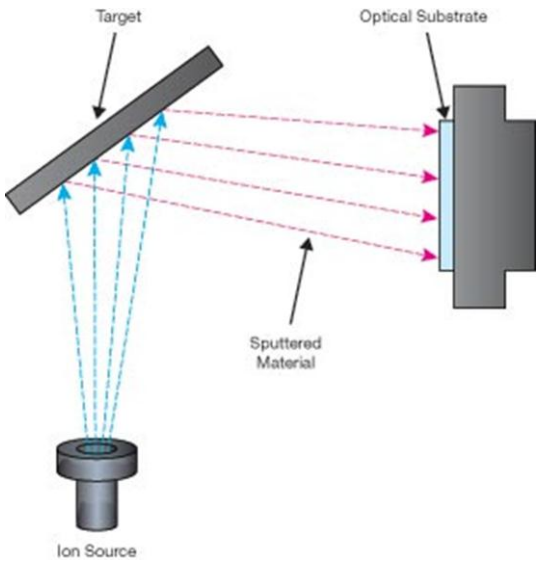

Figure 3-3: Ion beam sputtering; material is removed from the target by a stream of high velocity ions [3].

Similar to a magnetron, an ion beam sputter system (Figure 3-3) ejects material from a target using accelerated ions. In an ion beam system, however, the ion source is physically separated from the target. Plasma is generated in a small chamber and the ions produced are accelerated and ejected from the chamber using a charged grid. Since the accelerating field does need to penetrate the target, an ion beam system can be used with conducting or insulating materials; an ion beam will sputter any target placed in front of it. Ion beam systems also operate at a lower chamber pressure which can improve film quality and the ion beam configuration permits independent control of ion flux and ion energy. The downside of this type of tool is the need for frequent maintenance of the filaments and grids. Because of this high maintenance requirement, ion beam systems can be impractical for certain applications.

E-Beam Evaporator

Deposition of metal contact pads was performed with an electron beam evaporator (manufactured by Sharon Vacuum) at Harvard's CNS facility (Figure 3-4). This tool can deposit up to six different materials without breaking vacuum which makes it ideal for deposition of semiconductor contacts which often require that several layers of metal be deposited without exposure to air.

E-beam systems use a focused electron beam to vaporize target material. The vaporized material then deposits on all surfaces in the vacuum chamber[49]. The tool uses a cryo-pump to achieve a base pressure on the order of 10^{-7} Torr. This low pressure environment allows the tool to deposit high purity films.

Figure 3-4 One of the electron beam evaporators at CNS [2].

Rapid Thermal Processor

Rapid thermal processors (RTP) are commonly used in semiconductor processing to heat thin film materials. Many materials require heating to high temperature to alter their crystalline structure or to blend multi-layered materials. Dopants are added to semiconductors to increase the number of charge carriers in the material which increases the material's electrical conductivity. After the dopants are introduced, the material must be heated to allow the dopants to fully incorporate themselves into the crystal structure. The other common use for an RTP is in producing electrical contacts. Creating efficient electrical contacts on a semiconductor device can be quite challenging. It is often necessary to deposit several layers of metal on the semiconductor and then heat the metal stack to fuse the layers together.

For this project, the RTP at CNS was used to anneal electrical contacts. The "rapid" in rapid thermal processing made the tool particularly appealing. Heating in a conventional furnace can take hours, whereas an RTP can do the same job in minutes. With the need to process multiple samples, the RTP saved considerable time.

Tube Furnace

RTP annealing (above) works quite well for metallic contacts, but is insufficient for the post-deposition processing of TCO films. The TCOs used here, and TCOs in general, must be heated for considerable time (typically 1 hour) before the

material can develop the desired electrical and optical properties. Also, this post-deposition annealing often requires an oxidizing (or, in some cases, reducing) atmosphere.

The atmospheric pressure tube furnace at CNS was used for all TCO annealing. This tool can operate at up to 1100°C with a choice of gases flowing through the sample chamber. Nitrogen, argon, oxygen, and forming gas (95% argon, 5% hydrogen) are available for processing.

Profilometer

The Veeco Dektak 6M stylus profilometer ("the Dektak") is a metrology instrument used to measure film thickness (Figure 3-5). It moves a stylus across the surface of a sample and measures the deflection of the stylus to produce a profile map of the surface. Film thickness is measured by moving the stylus from a region of bare substrate (masked during deposition) to region covered by the deposited material. The Dektak at the Tufts Micro & Nano Fabrication Facility was used to measure TCO film thicknesses.

Figure 3-5: Dektak profilometer at TMNF

Ellipsometer

Ellipsometry is a non-destructive metrology technique used to determine the optical properties of thin films. It can determine transmittance, reflectance, and complex index of refraction as functions of wavelength. It can also produce very accurate and precise measurements of film thickness.

An ellipsometer produces a beam of light of known polarization, intensity, and frequency (see Figure 3-6). The beam is reflected off a material sample and

collected by a detector. The ellipsometer compares the known properties of the incident light with the measured properties of the reflected light to produce two quantities, Ψ and Δ. Ψ is the amplitude ratio of the incident and reflected beams and Δ is difference in polarization phase angles. From these two numbers, the system can derive the film thickness and optical constants.

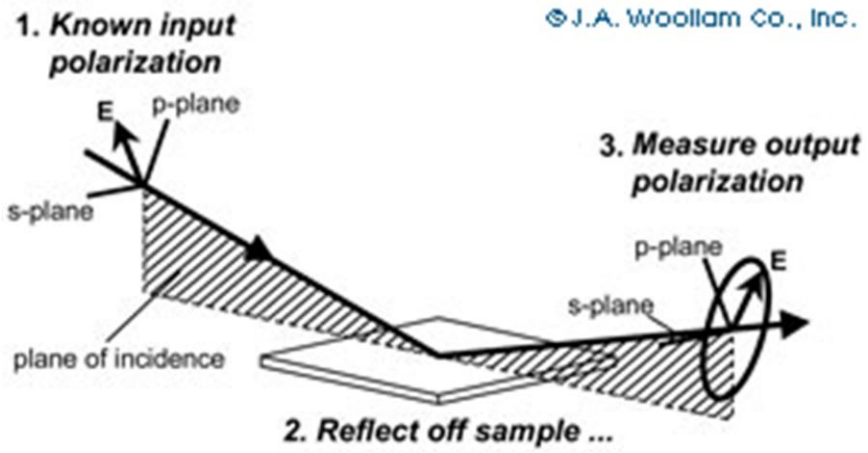

Figure 3-6: By reflecting light off a surface and measuring the change in polarization, an ellipsometer is able to determine the thickness and optical constants of a material.

Multispectral ellipsometers can take data over a range of wavelengths to produce a complete description of a material's optical response. Measurements are taken across a range of incident wavelengths and at several angles of incidence. With this large set of data, the modeling software can attempt to produce values for

the complex index of refraction at all measured wavelengths. The software also solves for the film thickness. Fitting an accurate model to the ellipsometric data requires an iterative solution method and is dependent on initial estimates of the film thickness and, depending on the model being used, possibly several other parameters. The uncertainties involved in choosing a model and making initial estimates of parameters can make data modeling very difficult but, when successful, multispectral ellipsometry provides a complete description of a material's optical behavior.

To determine the film thickness and the real index of refraction of a film deposited on a well characterized substrate, an ellipsometry software package will use know material property values (supplied by the user) combined with measured values of ψ and Δ. The software attempts to find simultaneous solutions to a set of reflectivity equations for all measured frequencies and incident angles. Starting with the "best guess" values for the thickness and index of the film (supplied by the user), the system will make repeated attempts to refine its model until it arrives at a model with the lowest attainable mean squared error (Figure 3-7).

The following system of equations describes the behavior of a polarized beam of light reflecting from a thin film deposited on a substrate. With enough data available, this system can be solved to produce very accurate values for n_1 (the real index of refraction for the film) and d (the thickness of the film).

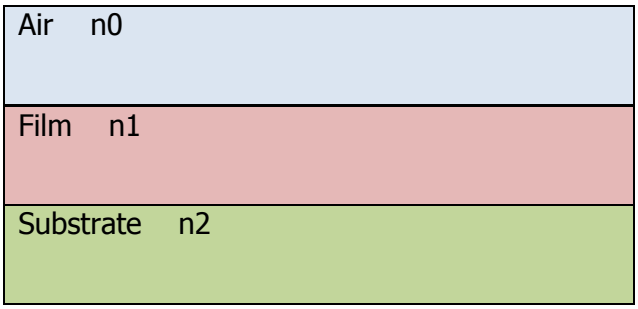

$$\tan\Psi = \frac{|R_p|}{|R_s|} \qquad \Delta = \delta_p - \delta_s$$

$$R_s = \frac{r_{01,s} + r_{12,s}e^{-2i\beta}}{1 + r_{01,s}r_{12,s}e^{-2i\beta}} = |R_s|e^{i\delta_s}$$

$$R_p = \frac{r_{01,p} + r_{12,p}e^{-2i\beta}}{1 + r_{01,p}r_{12,p}e^{-2i\beta}} = |R_s|e^{i\delta_p}$$

$$r_{01,s} = \frac{n_0\cos\phi_0 - n_1\cos\phi_1}{n_0\cos\phi_0 - n_1\cos\phi_1} \qquad r_{01,p} = \frac{n_1\cos\phi_0 - n_0\cos\phi_1}{n_1\cos\phi_0 - n_0\cos\phi_1}$$

$$r_{12,s} = \frac{n_1\cos\phi_1 - n_2\cos\phi_2}{n_1\cos\phi_1 - n_2\cos\phi_2} \qquad r_{12,p} = \frac{n_2\cos\phi_1 - n_1\cos\phi_2}{n_2\cos\phi_1 - n_1\cos\phi_2}$$

$$\beta = 2\pi\left(\frac{d}{\lambda}\right)n_1\cos\phi_1$$

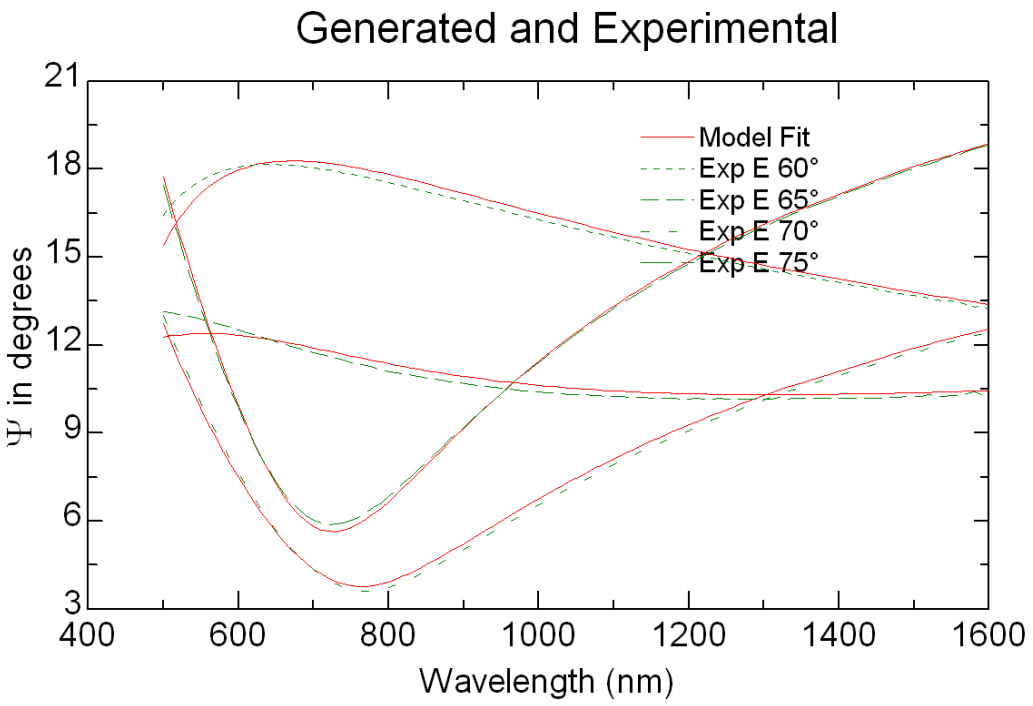

Figure 3-7: Measured values of psi (green) and the best fit generated by modeling software (red) for a sample of semiconductor; the fit is quite good except at the lowest wavelengths where the material is approaching its band gap.

For this research, the values of optical material properties were determined using a VASE (Variable Angle Spectroscopic Ellipsometry) Ellipsometer made by J.A. Woollam Co. The analysis described above assumes that the film in question exhibits no absorption of light for any frequencies being tested. It also describes a single film that displays uniform properties throughout and has no surface defects. The VASE system uses a much more sophisticated software package which can provide values for the complex index of refraction, which allows for

accurate analysis of absorbing materials. The VASE system can also be used to study multiple layers, non-uniform films, and films with rough surfaces.

Hall Effect System

The electrical properties of material samples were measured with the MMR Technologies K2500 Hall effect measurement system at the Center for Nanoscale Systems (Figure 3-8). The Hall Effect system can measure resistivity, carrier concentration, and carrier mobility.

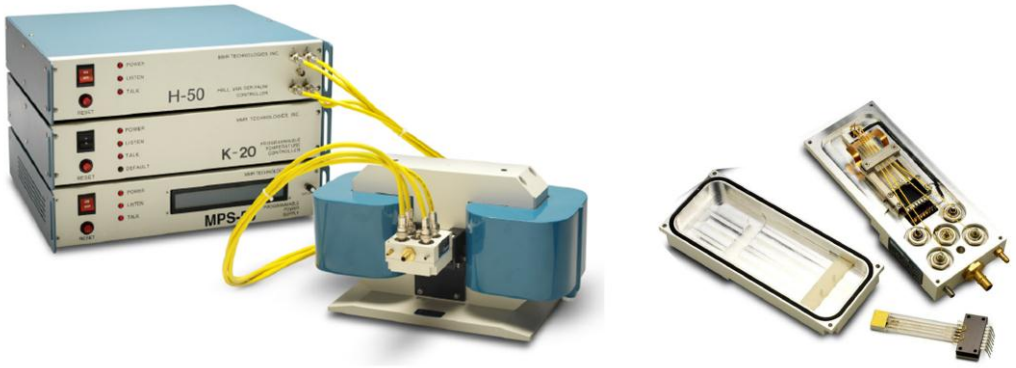

Figure 3-8 Hall effect measurement system and the sample chamber [1]

The Hall Effect occurs when a current is passed through a conductive material in the presence of a strong uniform magnetic field (Figure 3-9). With the current and magnetic field arranged perpendicularly, the charge carriers will be deflected from the direction of current flow and charge will accumulate at the edge of the

material sample. These charges create a potential difference across the sample and charge will continue to accumulate until this potential becomes strong enough to repel any new charge carriers. This competition between the magnetic field and the induced potential will bring the system to an equilibrium state with a constant induced potential[41, 51].

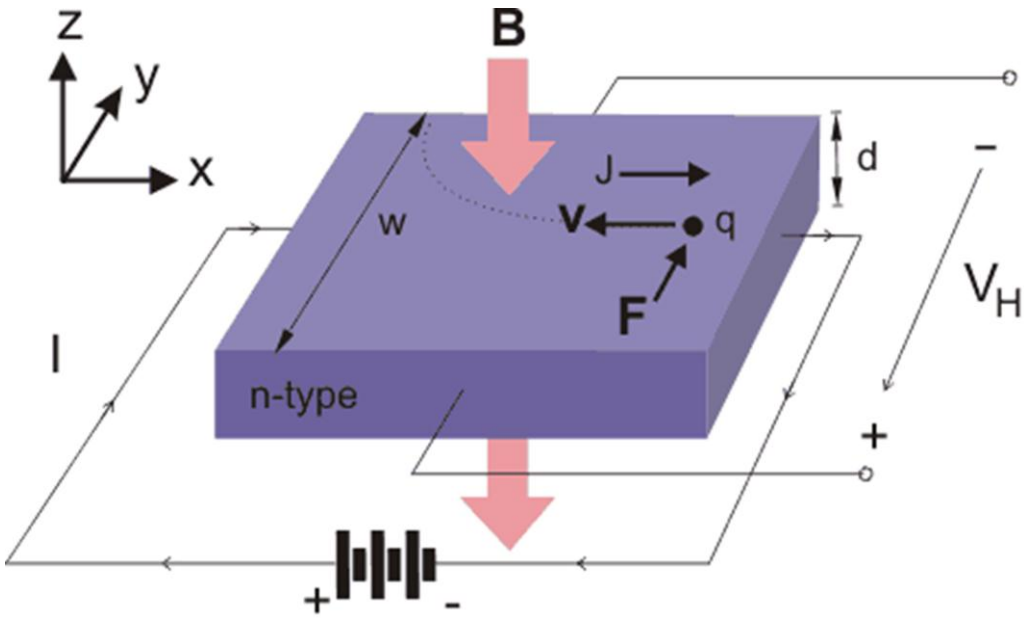

Figure 3-9: The Hall Effect: a carrier with charge q and velocity v is deflected by a force F induced by the applied magnetic field B causing charge build up which produces the Hall voltage V_H [5].

Using a four point probe arrangement, the system first performs a Van Der Pauw resistivity measurement to determine the sheet resistance (R_S)[52]. It then performs a Hall measurement and records the current (I) and the induced

potential, the Hall voltage (V_H). The applied magnetic field (B) is known. With these quantities, the system can then calculate[53, 54]:

$$carrier\ sheet\ density, \qquad n_s = \frac{IB}{q|V_H|}$$

$$majority\ carrier\ mobility, \qquad \mu = \frac{1}{qn_sR_s}$$

Chapter 4 – Rebuild of Ion Beam Sputter Tool

Initial Condition

As previously discussed, ion beam sputter systems can deposit a wide variety of materials and they operate at a relatively low chamber pressure. These properties allow ion beam systems to produce high quality films from oxide targets, which makes them an excellent choice for the deposition of TCOs.

The university owns an ion beam sputtering system (Figure 4-1) which is located at 4 Colby Street in the laboratory space shared by Professors Vandervelde and Hopwood. The tool had been unused for several years and was in very poor condition; many components were missing and, as would be learned, none of the remaining components were functioning properly. The tool clearly needed a great deal of work, but after considering its potential value,

Figure 4-1: Ion beam deposition system.

the decision was made to rebuild it. Work began on the ion beam system in the summer of 2009.

As built (by Sharon Vacuum), the tool was an ion beam sputtering system (as described in Chapter 3) with the following features:

- Quartz crystal deposition monitor
- Liquid cooling for cryo-pump, thickness monitor, and chamber walls
- Mass flow control system for the argon supply
- Multi-channel pressure monitor
- Thermocouple, capacitive manometer, and ion gauge pressure measurement in the chamber
- Thermocouple pressure measurement in the cryo-pump
- System interlocks to prevent damage to cryo-pump and ion source
- Cooled target holder for four targets
- Heated and rotating substrate holder
- Substrate shutter
- Two stage (mechanical and cryo) pumping system
- Front panel controls for all sub-systems
- Manually controlled throttle between chamber and cryo-pump
- Secondary ion beam for ion assisted deposition

Rebuild

An initial assessment of the tool showed several missing components and wiring and tubing in poor condition. More problems were discovered over time. The following is a partial list of the missing or damaged components:

- No documentation for system or any components
- Rough pump disconnected
- Vacuum lines missing
- Compressed air lines missing
- No cooling system
- Wiring and tubing tangled
- Improper grounding for electronics
- Vacuum valves missing, not working, or leaking
- Actuators for vacuum valves missing or not working
- Wiring for actuators severed
- Cryo-pump low on helium
- Gas flow control system missing
- Ion source dirty and missing filaments
- Substrate holder missing
- Substrate shutter not working
- Thickness monitor not working
- Capacitive manometer not working

The first task was simply to supply the system with power, compressed air, and coolant, all of which are needed for routine operation. The tool was already hardwired to a dedicated circuit; a single power line feeds the tool's electrical panel. With the tool hardwired to the wall, it would have been difficult to move, but this was not necessary as it was already placed in an ideal location in the laboratory. It was, and is, near a wall that separates the lab space from a service alley. Lines were run from the service alley to connect the tool to the building's supply outlets for compressed air and glycol coolant. New manifolds and supply lines were added to make all needed connections. The fluid in the mechanical vacuum pump was replaced and the pump was placed in the service alley to reduce noise in the lab space. New vacuum tubing and fittings were installed to connect the pump to the chamber and the cryo-pump.

The wiring was untangled, bad wiring was replaced, and all electrical components were grounded. The wiring and tubing were bundled and secured to prevent accidental damage.

The tool's vacuum valves are controlled by compressed air with the air supply controlled by solenoid valve actuators. Most of these actuators were missing or inoperative so new ones were installed. It was then possible to test the vacuum valves. Two of them did not work; the pistons had frozen in place after years of disuse. After disassembly and lubrication they moved freely.

At this point it was possible to test the rough pumping ability. The chamber was pumped out with the mechanical pump and the pressure measured with the

chamber's thermocouple gauge. All components worked well, and the chamber held vacuum quite well; in later tests with the cryo-pump it was able to hold sub-millitorr pressure overnight and sub-torr pressure indefinitely.

The pressure gauge on the cryo-pump compressor was reading below the manufacturer's recommended level, which meant it would be necessary to recharge the helium-4 refrigerant. Changing or topping off the gas in a helium compressor can be a delicate operation. The gas in the compressor must be kept as pure as possible (99.999% recommended), so all possible precautions must be taken to prevent contamination during maintenance. Before recharging, the helium filter was replaced. A tank of 99.999% pure helium and a new high-purity regulator were purchased. The gas supply was connected the compressor with clean stainless steel tubing with a tee fitting to connect the line to a high vacuum source (a turbo pump system). After leak testing the line, the vacuum source was turned on and left overnight to pump out the line. With the line cleared, the vacuum source was valved off, the supply tank opened, the compressor's inlet valve opened until the desired pressure was achieved.

With the cryo-pump now working, the complete pumping system was tested. The cryo-pump, the large gate valve (with new actuator and supply lines) connecting the cryo to the chamber, and the chamber ion gauge all worked well. The chamber can be pumped from atmosphere to under ten micro-torr in fifteen minutes and will achieve a base pressure on the order of 10^{-8} torr in a few hours.

The plasma chamber at the center of the ion source requires a precise and constant flow of high purity argon to sustain the plasma. An entirely new gas supply system was built from used, but serviceable, parts. Starting at the supply tank (99.999% pure argon), the gas flows through a regulator, cleaned stainless tubing, a mass flow controller, and a vacuum valve before entering the chamber through the back of the ion source. The mass flow controller and the valve are operated from the tool's main panel.

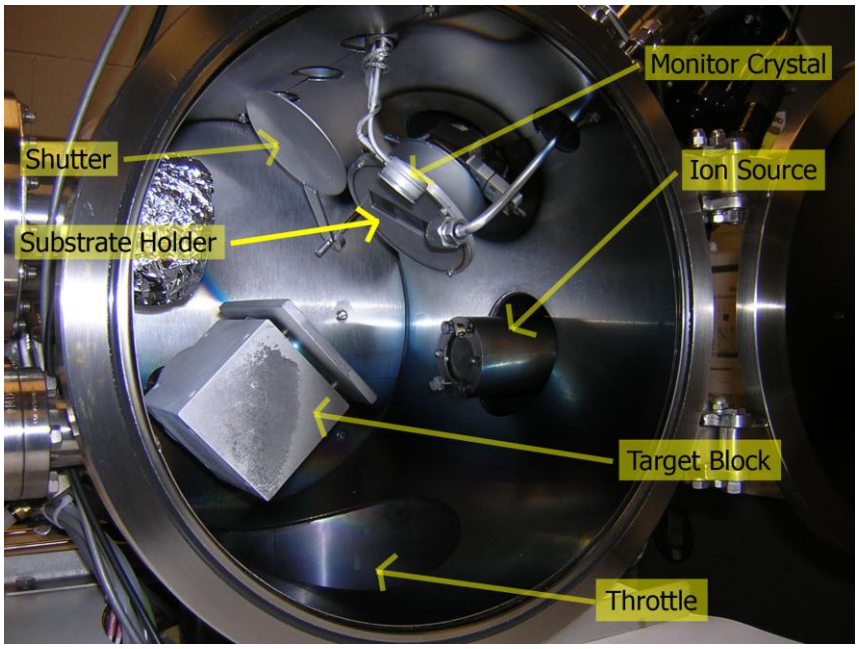

Figure 4-2: Chamber of ion beam tool.

A new substrate holder was designed and the parts were machined from stainless steel. It can hold a 2" wafer, a 4" wafer, or a glass microscope slide. The components are shown in Figure 4-2, See Appendix 2 for the drawings. The

substrate shutter was inoperative, but replacing the actuator and correcting an improper connection solved the problem.

The control unit for the thickness monitor was replaced, as were the capacitive manometer and its control unit. With these last items corrected, the tool was, in theory, fully restored. In fact, a much more difficult problem remained to be solved.

Low Beam Current

With all sub-systems repaired, the full system was tested, but the ion beam would not start. The anode in the ion source looked dirty (Figures 4-3 and 4-4), and so, the source was disassembled for cleaning. The metal parts from the plasma chamber were cleaned in a bead blaster (as recommended by the manufacturer) and the accelerator grids were gently cleaned by hand. After reassembly the ion beam started easily and the system seemed to work properly for a few days.

Figure 4-3: Plasma source base and cathode before cleaning.

Figure 4-4: Plasma source base and anode before cleaning.

Further testing showed erratic performance; system performance was often inconsistent from day to day. Also, the electron current through the ion generating plasma (anode current) was significantly lower than the figures quoted in the power supply and ion source manuals resulting in a consistently low deposition rate. The ion source was sustaining a plasma, but it was not sufficient to generate the desired ion beam. The most likely causes of low anode current in this type of ion source are i) dirty anode, ii) poor cathode current, or

iii) poor gas flow or contaminated gas. These and other possible causes were investigated, but the problem persisted. The following tests were performed:

- Conductivity tests on all electrical pathways.
- Short circuit tests between all electrical pathways. Some very small shorts were found. These were corrected by removing the ceramic insulators from the ion source and cleaning them in acid to remove metallic contamination.
- Argon supply to ion source tested for flow rate.
- Argon supply to ion source tested for vacuum integrity. No leaks detected, which would indicate that the argon is not being contaminated by outside air.
- Verified calibration of thickness monitor.
- Cathode current verified.
- Surface conductivity of anode cylinder tested.
- Ion source tested at a variety of power supply settings.
- Ion source tested at a variety of gas flow rates.
- Chamber lining panels removed and cleaned.

During the testing of electrical pathways, several of the circuit boards in the ion beam power supply were removed and it was observed that two of the board connectors were loose. After reinstalling the boards, the issue of the erratic system behavior resolved itself for a few days. When the erratic performance

returned, it became clear that the power supply needed to be replaced or repaired. Repairing the unit would be a fraction of the cost of replacement, so it was shipped to Advanced Energy for repairs. When it was returned and reinstalled, the erratic system behavior was eliminated, but the low deposition rate remained.

Throughout the repair process, tech support staff at Advanced Energy were very helpful; they gave useful instruction for testing of the power supply. The ion source was made by Commonwealth Scientific, Inc. which was purchased by Veeco in 2000. Veeco tech support confirmed that the anode current was lower than would be expected and, after reviewing previous test results, a conclusion was reached that the only thing left to try was a replacement of the magnets around the plasma source. These strong permanent magnets produce a uniform magnetic field which causes electrons in the plasma to gyrate around the field lines on their way from the cathode to the anode thereby increasing their effective path length which increases the likelihood of an ionizing collision with an argon atom. This technique increases plasma density and allows for a higher beam current. If the magnets had degraded, it would explain a weak beam current. New magnets were ordered, but their installation produced no change in performance.

The same technician from Veeco reviewed the existing operating procedure (taken from the equipment manuals) and suggested some changes including

slightly lower power settings and a higher gas flow rate. With the new power supply and new operating procedures, the tool performs reliably.

Secondary Ion Beam

As built, the system included a second, gridless, ion source for use in ion-assisted deposition. The source faces the substrate and bombards the substrate surface with argon ions during deposition. The added energy alters the structure of the deposited material.

The gridless source and its power supply were in storage; reinstallation was fairly simple. Unfortunately, the power supply is not working properly. This power supply has integrated controls for all ion source operations including gas flow control. The flow control circuit is completely inoperative and the power supply will not function without it. Interestingly, the case fan is also not working; it is not getting any power. If both problems are caused by a failure in an internal low voltage supply, then it may be possible to repair the unit inexpensively.

DC Magnetron

With the secondary ion source inoperative, there was a large feed through port available in the chamber. A 3" DC magnetron was installed in the opening with the intention of using the ion beam and the magnetron simultaneously to perform co-sputtering depositions. The magnetron works well and deposits

aluminum at a rate of 2.7 angstroms per second at a very conservative operating power level.

The magnetron and the ion beam can be operated together but the chamber pressure must be maintained above the ideal operating pressure for the ion beam (10^{-3} torr instead of 10^{-4}). This increased argon pressure causes dispersion in the ion beam which lowers the sputtering rate and, possibly, effects film quality. A much more pressing concern is that the magnetron and the ion source face directly at each other so the magnetron will deposit large amounts of material onto the accelerator grid of the ion source. For this reason the current configuration should not be used for co-sputtering.

Current Status

The ion beam deposition system at 4 Colby Street is fully operational and can deposit aluminum at a rate of 1.0 angstrom per second at the maximum recommended power settings. Performance with other materials has not been determined.

The DC magnetron is still in place and fully operational. The secondary ion source awaits repairs.

Chapter 5 – Results

This chapter details the experimental results for the fabrication of a transparent conducting oxide (TCO) and associated antireflective coating using a minimal amount of rare-earth materials. The first requirement for the contact system is the fabrication of a high performance conducting layer. As expected, this requirement has proved to be very challenging.

Dozens of TNO samples have been produced and tested, and none have shown the expected conductivity. The samples were annealed in various atmospheres (N_2, O_2, Ar, Ar/H_2) at various temperatures (from 250°C to 550°C). A variety of contact materials have been tried (Au, Ti, Al, Cr, Ni). It now seems that this emphasis on post-deposition processing was a mistake. A recent review of the current literature suggests that the problem was with the deposition itself. All deposition to date has been conducted in a pure argon environment, and this appears to be the critical factor. The deposition for a conducting oxide should be conducted in a mixture of argon and oxygen[17].

The next attempt to produce a TNO conducting layer will use oxygen during deposition. If this solves the problem of poor conductivity, then work can begin on the proposed antireflective layers. It has often been said that one learns more from failure than success; here, much has been learned. The extensive

work on the post-processing aspects of TCO production and material analysis has laid the ground work for the Ph.D. phase of research.

TCO Optical Properties

Optical properties of TNO samples were measured using multispectral ellipsometry (discussed in Chapter 3). The results for a typical sample are presented.

The values of the raw data, Δ and ψ, along with the model curves that were fit to that data are shown in Figures 5-1 and 5-2. Measurements of Δ and ψ were taken for wavelengths from 300nm to 1600nm but the data below 500nm had to be deleted to produce a working model. As can be seen in the graphs, the model fit is quite good in the infrared region but there are some small deviations in the visible portion. It was increasingly difficult to fit data at lower wavelengths and no fit could be made to the data below 500nm. The material, as deposited, seems to have complicated optical behavior in the visible region. This is possibly due to poor homogeneity in the material. Improved deposition procedures may produce better results.

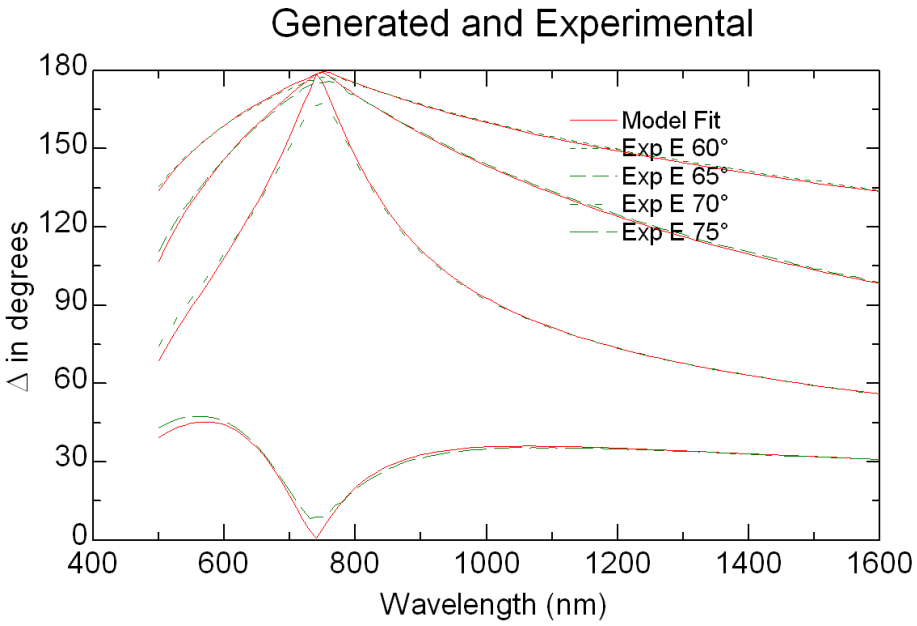

Figure 5-1: Model of optical behavior of TNO sample. Experimental values of Δ (green) and the best fit model (red).

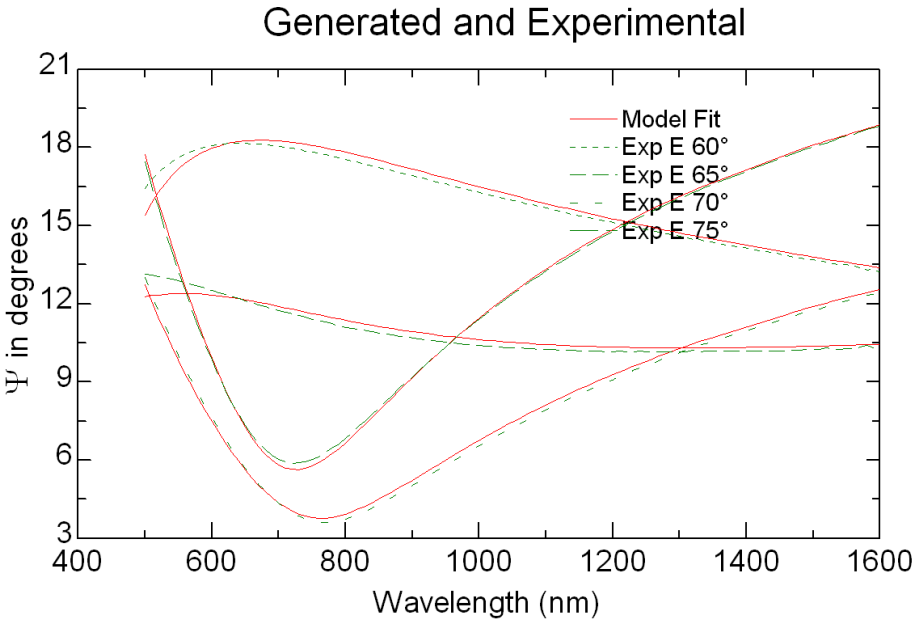

Figure 5-2: Model of optical behavior of TNO sample. Experimental values of ψ (green) and the best fit model (red).

This model was used to produce the optical constants for the TNO sample. The value of the real index of refraction, n, is shown in Figure 5-3. The model produces a real index value of about 2.35 at 600nm. This is consistent with values reported for TNO and TiO_2. The remaining values on the curve are consistent with data published for TiO_2; no such data has been published for TNO. The data for the extinction coefficient, k, is not shown; k was near zero for all wavelengths.

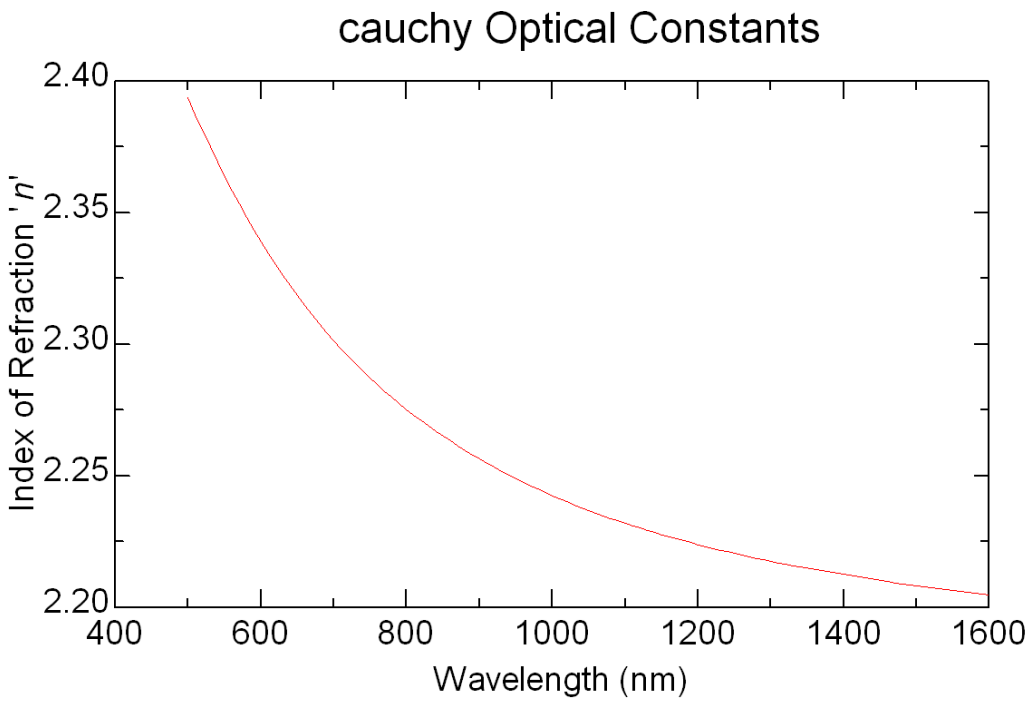

Figure 5-3: The real index of refraction for a TNO sample.

TCO Electrical Properties

Electrical properties of TNO samples were measured using a Hall Effect system (discussed in Chapter 3). Most samples tested showed little or no conductivity. The results for the best sample, with three different contact materials, are presented.

Contact pads were deposited on three pieces of the TNO sample using chrome, titanium, and aluminum. 100nm of the metal was deposited and then capped with 100nm of gold. The contacts were annealed at 200°C for 30 minutes in a nitrogen atmosphere.

All measurements were made under vacuum and at room temperature (300K). The Hall Effect system was operated with a magnetic field strength of 1.3T and the maximum voltage applied to each sample was 2.0V.

The result are shown in Table 5-1. Keeping in mind that the goal is to produce a conductor to replace ITO, which has a resistivity on the order of 10^{-4} Ωcm, these results will need to be improved considerably. The system also indicated that the samples showed poor uniformity; the system measures resistivity in four different directions across the sample and these measurements varied from one another by more than 10%. Clearly the deposition procedure needs updating, but we are quite confident that the change in deposition atmosphere will produce the desired results.

Contact Metal	Carrier Type	Carrier Concentration [cm^{-3}]	Carrier Mobility [$cm^2/V/s$]	Hall Coefficient	Resistivity [Ωcm]
Cr	n-type	$2.5x10^{16}$	1000	245	0.238
Ti	n-type	$1.6x10^{16}$	287	386	1.340
Al	n-type	$7.8x10^{15}$	1423	796	0.559

Table 5-1: TNO electrical properties measured with Hall Effect system.

Chapter 6 – Future Work

Efforts to date have focused on producing a high performance TCO using available resources. Future work will incorporate antireflective treatments to create a complete top contact system.

Moth's Eye

Many nocturnal predators are able to detect their prey by looking for flashes of light reflected from the glossy surface of the prey's eyes. To evade these predators, moths have developed a very effective broad-spectrum antireflective coating on their eyes and wings. As reported by Bernhard in 1967 [55], this coating is formed from a hexagonal pattern of small cones (Figure 6-1). These structures are at a 200nm scale; the cone height and spacing between peeks are both approximately 200nm. Photons in the visible and infrared region of the spectrum are not able to interact with individual cones because the cones are smaller the wavelength of the photon and therefore must interact with the surface as a continuous medium. The conical structures effectively form a graded index material between the air and the bulk material. In this way, sub-wavelength scale structures are able to alter the perceived bulk properties of a material.

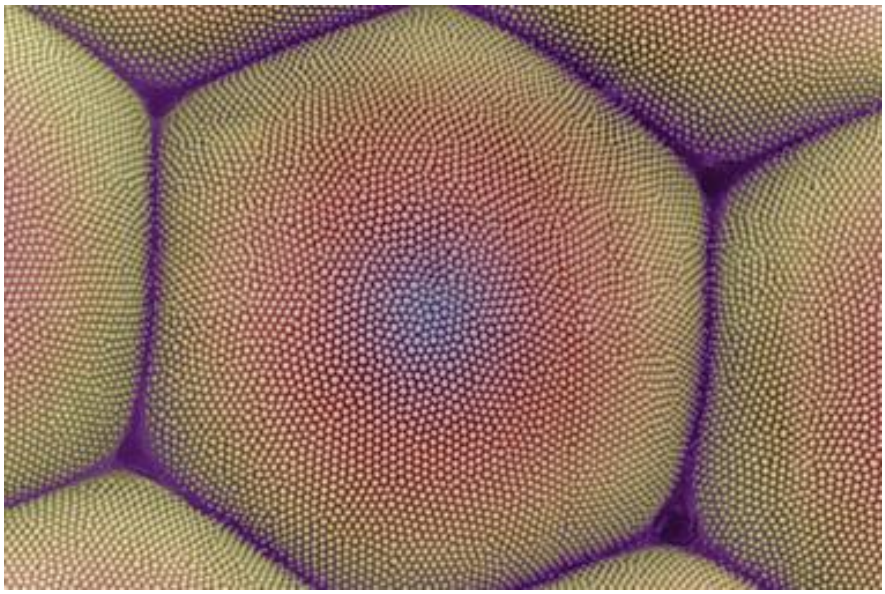

Figure 6-1: The surface of a moth's eye; a coating of sub-wavelength cones reduces reflection of visible light helping the moth to evade detection by predators[Newscom].

In the time since the first reports of this type of phenomena, tools have become available that allow the fabrication of synthetic versions of moth's eye and other sub-wavelength scale structures. The relentless efforts of the semiconductor industry to produce smaller transistors has been responsible for the development of a wide variety of tools designed for nano-scale fabrication.

A variety of techniques have been employed to fabricate these structures. Top-down methods, which remove material to form the cones, include UV lithography[56], electron beam lithography[57], and imprinting[58]. The lithography techniques remove material using a wet etch in an acid or solvent or a dry etch in a reactive ion etching system. Imprinting stamps the pattern into a

soft material (plastic). Bottom-up techniques, which grow the cones on the bulk material, have also been demonstrated[59].

These fabrication methods have been used to produce antireflective coatings on a wide variety of materials (dielectric oxides, semiconductors, polymers). These coatings demonstrate substantial improvements in optical transmission across the visible and IR spectrum[20].

Fabrication

Currently available publications suggest that introducing oxygen to the sputtering chamber during TNO deposition should increase conductivity to the desired level ($<10^{-3}$ Ωcm). With an effective conductor in place, work can begin on the antireflective layers.

In the proposed device, a layer of pure TiO_2 will be deposited on the TNO conductive layer. Since TiO_2 and TNO are nearly the same, differing only by the small addition of the niobium oxide dopant in TNO, they should form a nearly seamless optical transition. As the TiO_2 is deposited it will gradually be replaced with SiO_2 until pure glass is being deposited. This can be accomplished by depositing the materials in a system that uses two RF magnetron guns. The gun holding the TiO_2 target is started at full power and the power is slowly ramped down while the gun holding the SiO_2 gun is slowly ramped up.

This method does have an inherent difficulty; a magnetron gun requires a minimum power level to maintain a plasma which means that there is a minimum deposition rate. It is hoped that this will be a minor difficulty and will not prevent the fabrication of an effective ARC. Chemical vapor deposition (CVD) could also be used to deposit this ARC layer, but the precursor gasses would be problematic. The precursor for SiO_2 is silane and the precursor for TiO_2 is titanium tetrachloride. Both gasses are highly toxic, silane has a tendency to explode, and titanium tetrachloride is ruinously expensive.

At this point in the fabrication, the device will terminate with a pure glass (SiO_2) layer. To reduce reflection at the interface between air (n=1) and glass (n=1.4), a pattern of sub-wavelength scale (200nm) cones will be etched into this surface to provide a gradual optical transition from ambient air to the top layer of the device. This is moth's eye coating discussed previously. The method of fabrication for this layer is still being considered.

If this system works as proposed, it will provide an effective and sustainable top contact for wide spectrum photovoltaic devices.

Appendix 1

SOP for Ion Beam Deposition System

Sharon Ion Beam Sputter Tool

Standard Operating Procedure

Revised: June, 2011

Contacts:

Faculty Supervisor: Prof. Thomas Vandervelde, Electrical & Computer Engineering 617-627-5126

Tufts Emergency Services: 66911 from campus phone, 617-627-6911 from cell phone, or call 911

Primary Contact for Tool Operation: John Chivers, usually found in SciTech 217, john.chivers@tufts.edu, 617-627-2704

Warnings!

The tool uses high voltage and strong vacuum during deposition.
The ion beam power supplies produce **High Voltage**. Use caution when working around this tool.
Do not attempt to open the chamber until the ion beam power supplies are turned off, the cryo-pump gate valve is closed, and the ion source has cooled.
If you are unsure about any procedure, ask for help.

Required Checkout

You must have permission from the faculty supervisor before you may use this tool unsupervised. When you are first learning procedures, work with experienced lab users (students, post docs, faculty or staff) to become familiar with the tool.

Material Requirements

Equipment: substrate, targets
Personal protective equipment: safety glasses, nitrile gloves, Tyvek coat

Procedure

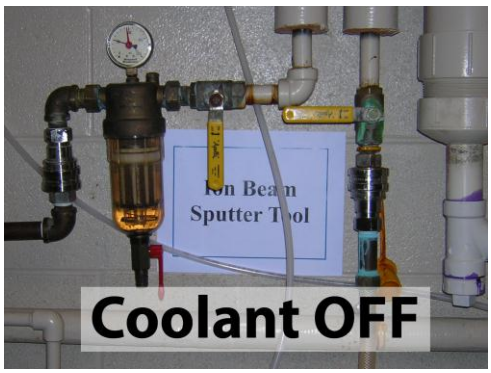

Turning the Tool On

1. Turn on the coolant using the **two** valves in the service ally. **Warning! The coolant must be flowing before the cryo-pump compressor is started. Without coolant the compressor will be damaged.**
2. Turn on the main power switch on the wall behind the tool.
3. Press the big green button on the Valve Control panel.
4. Turn on the mechanical pump by turning the switch at the left of the Valve Control panel. Wait a few minutes for the pump to clear out the roughing line.
5. Turn on the vacuum gauge controller.
6. The cryo-pump will probably be filled with gas that was captured during the last use of the tool. Clear this gas by opening the Regenerate Valve using the key on the control panel. The TC2 reading on the vacuum gauge controller shows the pressure in the cryo-pump. Wait until TC2 reads less than 50E-2, then close the Regenerate Valve.
7. Make sure the coolant is flowing!
8. Check the gauge on the back panel of the compressor. It should read 250 psi. If it shows any value lower than 248, do not start the compressor. Ask for help.
9. Turn on the cryo-pump using the switch on the front panel of the compressor.
10. The cryo takes about 1hr 45min to reach operating temperature. During this time you can load your targets and substrate.
11. The cryo is ready for use when the gauge mounted on the bottom of the cold head reads 15.

Working in the Chamber

1. Always wear gloves when working in the chamber.
2. Close the Throttle when working in the chamber.
3. Place the copper sheet on the bottom of the chamber to prevent screws or other debris from falling into the throttle. The copper sheet is stored in the small drawer across from the tool.
4. **Do not touch the ion sources**. The exposed filaments are fragile and must be kept clean. **Warning! After deposition the ion sources are hot.**

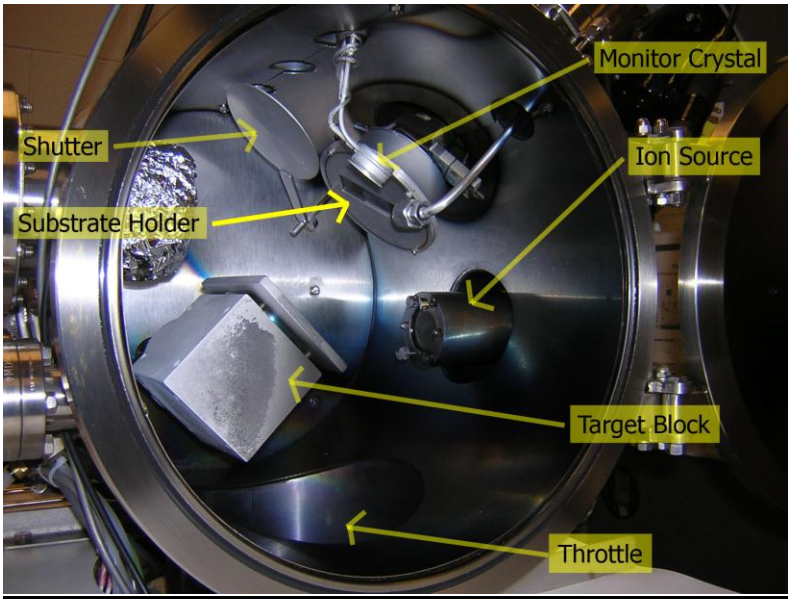

Opening the Chamber

Warning! Never open the chamber immediately after deposition. The ion source must be allowed to cool before being exposed to air.

Warning! Never open the chamber unless the valves to both vacuum pumps are closed.

1. Be sure the chamber is isolated from all other system components. All indicator lights on the Valve Control panel should be off (except for the mechanical pump).
2. To vent the chamber to air, open the valve on top of the chamber.
3. Open the door.
4. Close the valve on top of the chamber.

Changing the Targets

1. Follow all instructions listed under "Working in the Chamber."
2. The brackets that hold the targets are held down with four hex-head bolts. Use a 3/8" wrench.
3. The thinnest part of the bracket should be at the bottom when the target is facing the ion source.
4. Brackets and bolts are stored in a drawer opposite the tool.
5. The target block is rotated manually from the back of the tool.

Changing the Substrate

Substrate holders are available for 4" wafers, 2" wafers, and glass slides. Holders are stored in a drawer opposite the tool.

1. Follow all instructions listed under "Working in the Chamber."
2. Open the shutter. The shutter is controlled from the Sycon Thickness Monitor.
3. The substrate holder is held in place with four hex-cap screws. Carefully remove the screws using a 7/64" hex wrench and remove the substrate holder. The substrate assembly can be rotated using the Rotate button. Never remove the base of the substrate holder.

4. Mount your substrate.
5. Close the shutter.

Rough Pumping the Chamber

1. Remove the copper sheet.
2. Close the door.
3. Be sure the vent valve on the top of the chamber is closed.
4. Open the Throttle valve (metal handle with red knob).
5. All indicator lights on the Valve Control panel should be off except the Mechanical Pump.
6. On the Valve Control panel, press the Roughing button to open the roughing valve.
7. Leave the roughing valve open until you are ready to expose the cryo-pump.

Programming the Thickness Monitor

The Thickness Monitor must be reprogrammed for each material sputtered. The densities and z-factors for each target are posted on the tool.

1. Check the crystal life by pressing the LIFE button. If it reads below 50%, the crystal should be replaced; ask for help.
2. Press PROGRAM to enter program mode.
3. Cycle through the options by pressing ENTER.
4. Set the density and z-factor for the material you will be depositing. Do not change the tooling parameter (111%).
5. Press PROGRAM to leave program mode.

Switching to High Vacuum

1. **Close the roughing valve.**
2. **Do not open the High Vacuum valve unless TC1 reads less than 5.0E-2.**
3. All indicator lights on the Valve Control panel should be off except the Mechanical Pump.
4. Open the High Vacuum valve from the Valve Control panel.
5. The chamber will quickly pump down to 1.0E-5. It takes about 25min to pump to 1.0E-6. The ultimate base pressure in on the order of E-8. The tool does not require a low base pressure to sputter (1.0E-5 is fine), but a lower base pressure will improve film quality.

Starting Gas Flow

1. Turn off the ion gauge by pressing the "IG" button on the vacuum gauge controller.
2. Open the Argon tank valve.
3. Open the Argon line valve.
4. Open the Argon chamber valve by pressing the Argon button on the control panel.
5. Set the flow controller to AUTO. To do this, press the Valve button once, then press the up-arrow button to cycle through the options to AUTO, then press the Valve button again.
6. The mass flow controller is set for a flow rate of 10sccm (standard cubic centimeters per second). There is no need to change this.

Sputtering

1. Turn on Substrate Rotation.
2. Turn on the ID 2500 power supply.
3. Turn on the Source. Wait a few seconds.
4. Turn on the Beam.
5. Don't touch the other controls. Beam voltage should be 625V and beam current should be 25mA.
6. You may want to allow the beam to clean the target before sputtering. Materials that oxidize easily (Al, Cu, Ti) should be cleaned for at least 2 minutes. Gold should not need cleaning (don't waste gold!).
7. To begin deposition: press "Zero" on the thickness monitor and press "Open" to open the shutter.
8. When the thickness monitor reaches the desired thickness, close the shutter.
9. Turn off the Beam.
10. Turn off the Source.
11. Set the Argon flow controller to CLOSED.
12. Close the Argon chamber valve.
13. Turn off the ID 2500.
14. Close the High Vacuum valve.
15. Turn off Substrate Rotation.
16. **WARNING! DO NOT OPEN THE CHAMBER! The ion source must be allowed to cool before being exposed to air.**

Cooling the Chamber

1. After deposition, wait 10min with the chamber in vacuum.
2. Be sure the chamber is isolated from all other system components. All indicator lights on the Valve Control panel should be off (except for the mechanical pump).
3. Open the Nitrogen tank valve and the Nitrogen line valve.
4. Open the Vent valve for **20 seconds** (use a timer) by pressing the Vent button and then press it again to close. The Nitrogen will cool the Source without exposing it to oxygen.
5. Wait at least 30min, then open the chamber.
6. The Source will still be hot to the touch; don't touch it.
7. Alternatively, you can just wait 2 hour after deposition with the chamber in low vacuum (High Vacuum valve closed).
8. Open the chamber as described in "Opening the Chamber."

Turning the Tool Off

1. Close the chamber and pump it down to at least 5.0E-2.
2. Check that the Argon flow controller is set to CLOSED and the Argon chamber valve is closed.
3. Check the Substrate Rotation and Substrate Heater; they should be off.
4. The ID2500 should be off.
5. All indicator lights on the Valve Control panel should be off except the Mechanical Pump.
6. Turn off the cryo-pump compressor using the switch on its front panel.
7. Turn off the Vacuum Gauge Controller.
8. Close the line and tank valves for all gasses.
9. Turn off the mechanical pump then release the vacuum in the roughing line by opening the Roughing Line Vent Valve at the rear of the tool. Close the valve.
10. The only components that should still have power are the Thickness Monitor, Capacitive Manometer, and the Flow Control Meter.
11. Turn off the Main Power Switch on the wall.
12. Wait 5 minutes, then turn off the Coolant in the service alley. You should always let coolant circulate through the compressor after it is turned off.

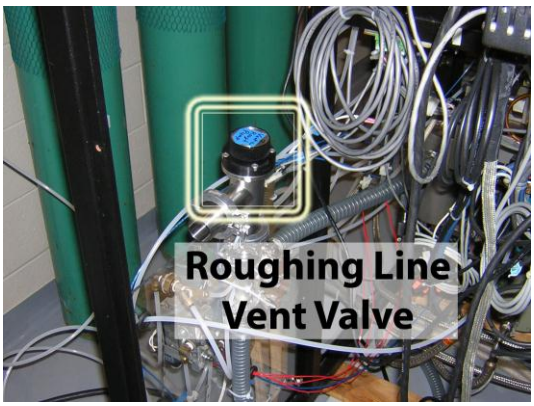

Notes on Vacuum Gauges

1. Thermocouple gauges are mounted in the chamber (TC1) and in the cryo-pump cold head (TC2). They are not very precise.
2. High vacuum pressure is measured by an ion gauge which will turn on automatically when the pressure is low enough. Do not turn on the ion gauge unless the chamber is under high vacuum. Exposure to higher pressure will damage the gauge.
3. Camber pressure can be monitored during deposition with the capacitive manometer. Close the manometer valve before venting the chamber. Do not expose the manometer to atmospheric pressure.
4. The accuracy of the ion gauge can be improved using the Degas feature.
5. The thermocouple and ion gauges are calibrated for Nitrogen (air), not Argon.

Appendix 2

Drawings of Substrate Holder for Ion Beam Deposition System

John Chivers
john.chivers@tufts.edu
617-519-0186

Base Plate

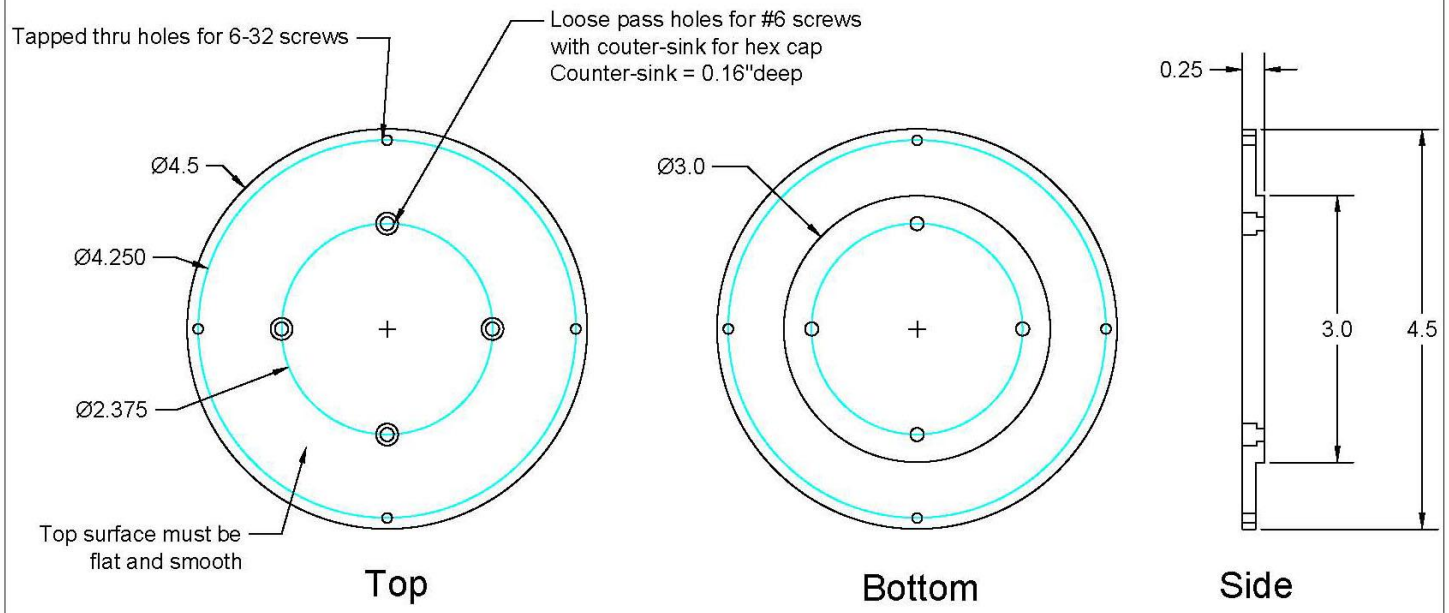

John Chivers
john.chivers@tufts.edu
617-519-0186

Ring with groove to hold 4" wafer

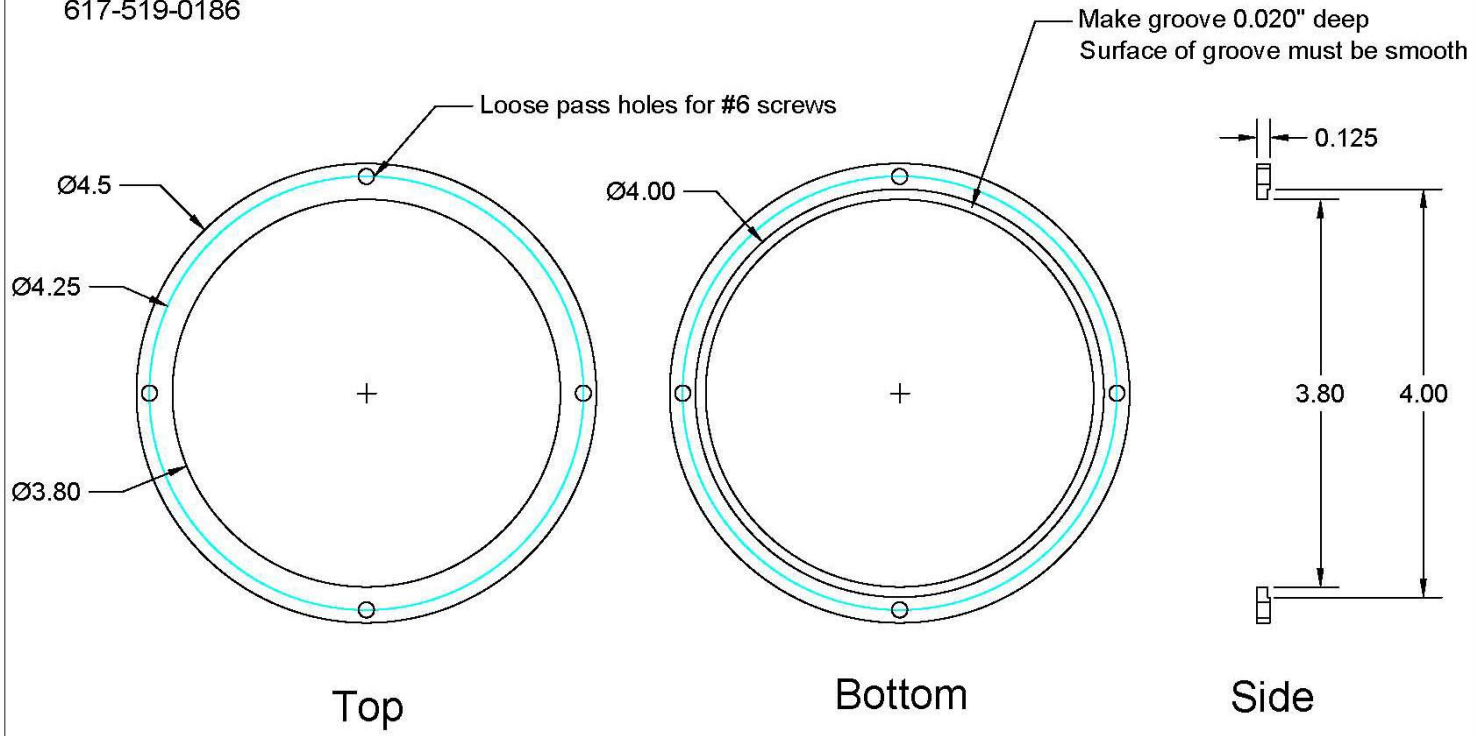

John Chivers
john.chivers@tufts.edu
617-519-0186

Ring with groove to hold 2" wafer

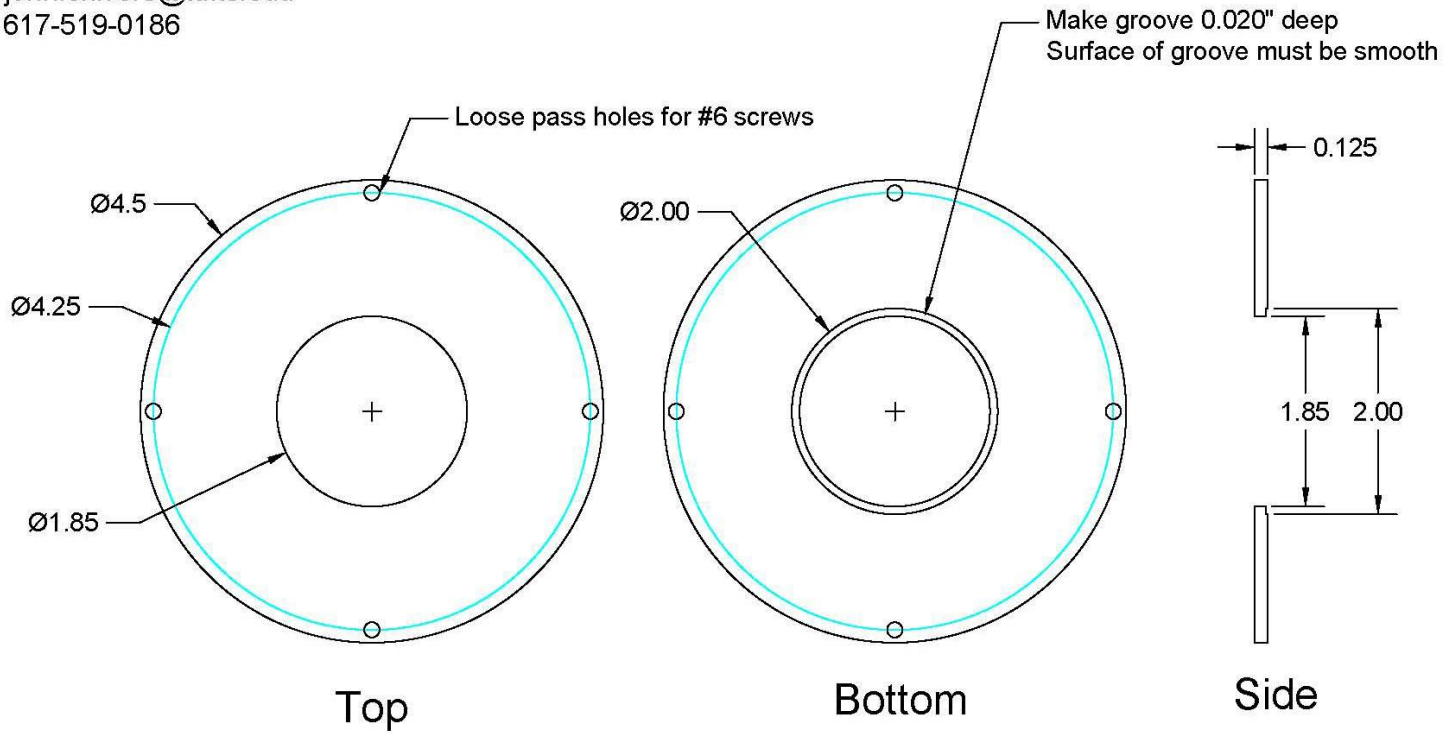

John Chivers
john.chivers@tufts.edu
617-519-0186

Disc with groove to hold glass slide

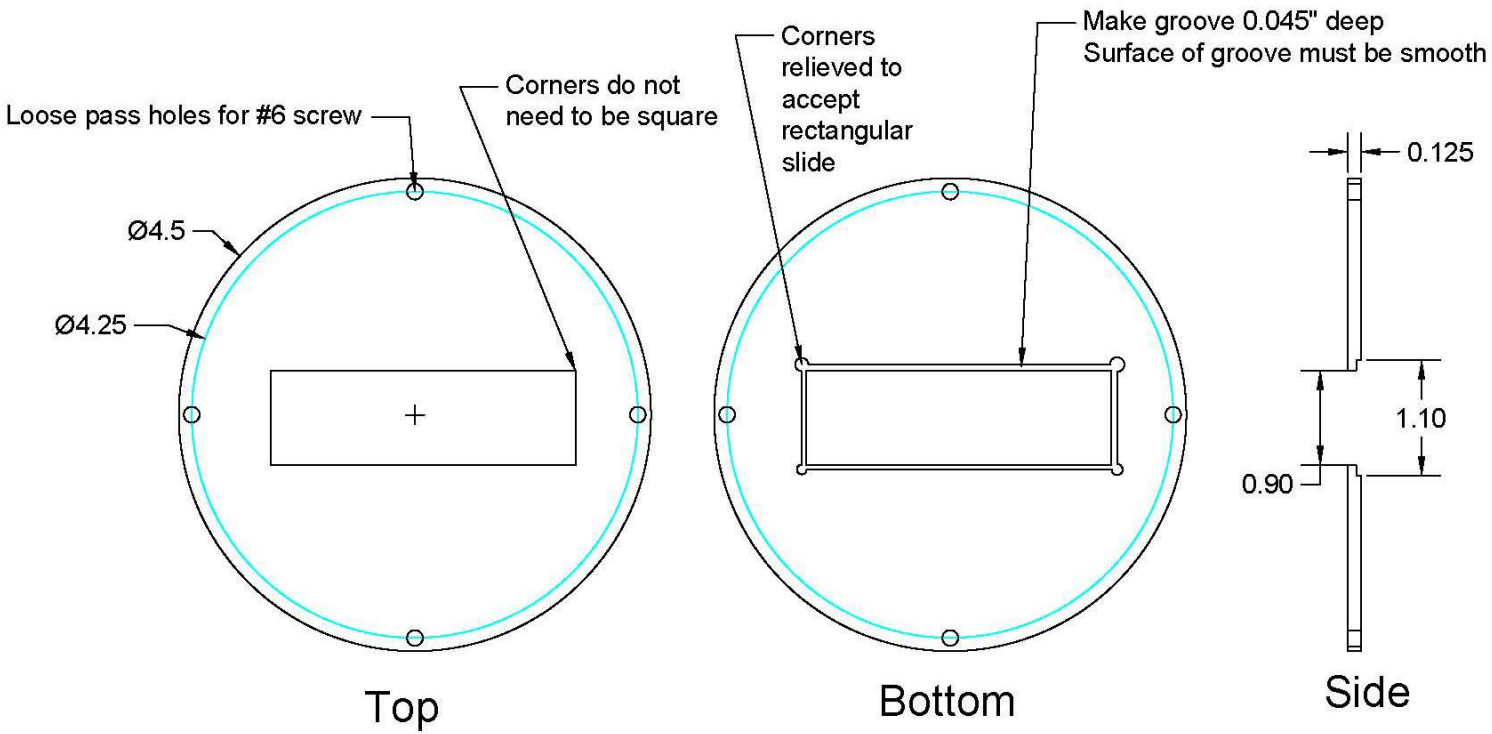

Sources

1. *MMR Technologies*. Available from: http://www.mmr-tech.com/.
2. *Center for Nanoscale Systems*. Available from: http://www.cns.fas.harvard.edu/.
3. *Lasertec, Inc.*; Available from: www.laserstec.com.
4. *D2 Inline Solutions*. Available from: http://www.d2inlinesolutions.com/index.html.
5. *Britney Spears' Guide to Semiconductor Physics*. Available from: http://britneyspears.ac/lasers.htm.
6. Razeghi, M., *Fundamentals of Solid State Engineering*2002: Kluwer Academic Publishers.
7. *SPECS Scientific Instruments*. Available from: http://www.specs-scientific.net/products/sputter-sources/sputter-source.htm.
8. Lewis, B.G. and D.C. Paine, *Applications and processing of transparent conducting oxides.* MRS Bulletin, 2000. **25**(8): p. 22-7.
9. Ginley, D.S., H. Hosono, and D.C. Paine, *Handbook of Transparent Conductors*2010: Springer.
10. O'Neill, B. *Indium market forces, a commercial perspective*. in *2010 35th IEEE Photovoltaic Specialists Conference (PVSC), 20-25 June 2010*. 2010. Piscataway, NJ, USA: IEEE.
11. Virolainen, S., D. Ibana, and E. Paatero, *Recovery of indium from indium tin oxide by solvent extraction.* Hydrometallurgy, 2011. **107**(1-2): p. 56-61.
12. Yoshimura, A., I. Dalgo, and Y. Matsuno, *Construction of global scale substance flow of indium from mining.* Nippon Kinzoku Gakkaishi/Journal of the Japan Institute of Metals, 2011. **75**(9): p. 493-501.
13. Zuser, A. and H. Rechberger, *Considerations of resource availability in technology development strategies: The case study of photovoltaics.* Resources, Conservation and Recycling, 2011. **56**(1): p. 56-65.
14. Fortunato, E., et al., *Transparent conducting oxides for photovoltaics.* MRS Bulletin, 2007. **32**(3): p. 242-7.
15. Sigdel, A.K., et al. *Superimposed RF/DC magnetron sputtering of transparent GA:ZNO with high conductivity for photovoltaic contacts applications*. in *35th IEEE Photovoltaic Specialists Conference, PVSC 2010, June 20, 2010 - June 25, 2010*. 2010. Honolulu, HI, United states: Institute of Electrical and Electronics Engineers Inc.
16. Saarenpaa, H., et al., *Aluminum doped zinc oxide films grown by atomic layer deposition for organic photovoltaic devices.* Solar Energy Materials and Solar Cells, 2010. **94**(8): p. 1379-1383.

17. Yamada, N., et al., *Transparent conducting Nb-doped anatase TiO2 (TNO) thin films sputtered from various oxide targets.* Thin Solid Films, 2009. **518**(11): p. 3101-4.
18. Brecl, K. and M. Topic, *Simulation of losses in thin-film silicon modules for different configurations and front contacts.* Progress in Photovoltaics: Research and Applications, 2008. **16**(6): p. 479-88.
19. Busani, T., et al., *Electrical and physical properties of room temperature deposited, mixed TiO2/SiO2 oxides.* Journal of Vacuum Science and Technology A: Vacuum, Surfaces and Films, 2006. **24**(2): p. 369-374.
20. Forberich, K., et al., *Performance improvement of organic solar cells with moth eye anti-reflection coating.* Thin Solid Films, 2008. **516**(20): p. 7167-70.
21. Boden, S.A. and D.M. Bagnall, *Optimization of moth-eye antireflection schemes for silicon solar cells.* Progress in Photovoltaics: Research and Applications, 2010. **18**(3): p. 195-203.
22. Ginley, D.S. and C. Bright, *Transparent conducting oxides.* MRS Bulletin, 2000. **25**(8): p. 15-21.
23. Badeker, K., *Conductivity and thermo-electromotive-force of some compounds of heavy metals.* Annalen der Physik, 1907. **22**(4): p. 749-766.
24. Huiyong, L., et al., *Transparent conducting oxides for electrode applications in light emitting and absorbing devices.* Superlattices and Microstructures, 2010. **48**(5): p. 458-84.
25. Gorrie, C.W., et al., *Effect of deposition distance and temperature on electrical, optical and structural properties of radio-frequency magnetron-sputtered gallium-doped zinc oxide.* Thin Solid Films. **519**(1): p. 190-196.
26. Furubayashi, Y., et al., *A transparent metal: Nb-doped anatase TiO2.* Applied Physics Letters, 2005. **86**(Copyright 2005, IEE): p. 252101-1.
27. Edwards, P.P., et al., *Basic materials physics of transparent conducting oxides.* Dalton Transactions, 2004(19): p. 2995-3002.
28. Exarhos, G.J. and X.-D. Zhou, *Discovery-based design of transparent conducting oxide films.* Thin Solid Films, 2007. **515**(18): p. 7025-7052.
29. Furubayashi, Y., et al., *Transport properties of d-electron-based transparent conducting oxide: Anatase Ti1-xNbxO2.* Journal of Applied Physics, 2007. **101**(9).
30. Coutts, T.J., D.L. Young, and X. Li, *Characterization of transparent conducting oxides.* MRS Bulletin, 2000. **25**(8): p. 58-65.
31. Gheidari, M. and E.A. Soleimani. *Study of Al/Ti, Al/Ni/Cr and Al/Mo ohmic contacts to indium tin oxide (ITO) for application in thin film solar cell*. in *ISES Solar World Congress 2007. Solar Energy and Human Settlement, 18-21 Sept. 2007*. 2007. Berlin, Germany: Springer-Verlag.
32. Kang, B.S., et al., *ITO/Ti/Au Ohmic contacts on n-type ZnO.* Applied Physics Letters, 2006. **88**(18): p. 182101-1.
33. Perkins, J.D., et al. *Optical absorption and electrical conductivity in amorphous In-Zn-O: a new TCO for CIGS PV*. 2009. Piscataway, NJ, USA: IEEE.

34. Perkins, J.D., et al., *Conductivity and transparency in amorphous In-Zn-O transparent conductors.* International Journal of Nanotechnology, 2009. **6**(9): p. 850-859.
35. Taylor, M.P., et al., *The remarkable thermal stability of amorphous In-Zn-O transparent conductors.* Advanced Functional Materials, 2008. **18**(20): p. 3169-78.
36. Yamada, N., et al., *Structural, electrical and optical properties of sputter-deposited Nb-doped TiO2 (TNO) polycrystalline films.* Thin Solid Films, 2008. **516**(17): p. 5754-7.
37. Yamada, N., et al., *Direct growth of transparent conducting Nb-doped anatase TiO2 polycrystalline films on glass.* Journal of Applied Physics, 2009. **105**(12).
38. Dabney, M.S., et al., *Pulsed laser deposited Nb doped TiO2 as a transparent conducting oxide.* Thin Solid Films, 2008. **516**(12): p. 4133-4138.
39. Gordon, R.G., *Criteria for choosing transparent conductors.* MRS Bulletin, 2000. **25**(8): p. 52-7.
40. Ginley, D., et al. *Next-generation transparent conducting oxides for photovoltaic cells: An overview*. 2001. San Francisco, CA, United states: Materials Research Society.
41. Anderson, B.L. and R.L. Anderson, *Fundamentals of Semiconductor Devices*2005: McGraw Hill.
42. Synowicki, R.A., *Spectroscopic ellipsometry characterization of indium tin oxide film microstructure and optical constants.* Thin Solid Films, 1998. **313-314**(1-2): p. 394-397.
43. Hecht, E., *Optics*. 3rd ed1998: Addison-Wesley.
44. Simmons, J.H. and K.S. Potter, *Optical Materials*2000: Academic Press.
45. Kasap, S.O., *Optoelectronics and Photonics, Principles and Practices*2001: Prentice Hall.
46. Busani, T. and R.A.B. Devine, *Dielectric and infrared properties of TiO2 films containing anatase and rutile.* Semiconductor Science and Technology, 2005. **20**(8): p. 870-875.
47. Devine, R.A.B. and T. Busani, *Molecular volume dependence of the electronic and ionic polarizabilities in TiO2 and SiO2.* Applied Physics Letters, 2005. **86**(6): p. 62902-1.
48. Lieberman, M.A. and A.J. Lichtenberg, *Principles of Plasma Discharges and Materials Processing*. Second ed2005: John Wiley & Sons, Inc.
49. Madou, M.J., *Fundamentals of Microfabrication*. Second ed2002: CRC Press.
50. Doering, R. and Y. Nishi, *Handbook of Semiconductor Manufacturing Technology*. Second ed2008: CRC Press.
51. Solymar, L. and D. Walsh, *Electrical Properties of Materials*. Seventh ed2004: Oxford University Press.
52. van der Pauw, L.J., *Method of measuring specific resistivity and Hall effect of discs of arbitrary shape*, 1958. p. 1-9.

53. Technologies, M. *Hall Effect Measurement System, Hall and van der Pauw Measurements*. Available from: http://www.mmr-tech.com/PDFs/hall_PPT.pdf.
54. Technology, N.I.o.S.a.; Available from: http://www.nist.gov/pml/semiconductor/hall_effect.cfm.
55. Bernhard, C.G., *Hur Naturen Lost Ett Svart Optiskt Problem (How Nature Has Solved a Difficult Optical Problem)*, in *Reprint: Hur Naturen Lost Ett Svart Optiskt Problem (How Nature Has Solved a Difficult Optical Problem).*1967: Sweden. p. 23p.
56. Heine, C., R.H. Morf, and M.T. Gale, *Coated submicron gratings for broadband antireflection in solar energy applications.* Journal of Modern Optics, 1996. **43**(7): p. 1371-1377.
57. Kanamori, Y., E. Roy, and Y. Chen, *Antireflection sub-wavelength gratings fabricated by spin-coating replication.* Microelectronic Engineering, 2005. **78-79**: p. 287-93.
58. Chen, Y., et al. *Soft nanoimprint lithography*. in *Advanced Microlithography Technologies, 8 Nov. 2004*. 2005. USA: SPIE - The International Society for Optical Engineering.
59. Sun, C.-H., P. Jiang, and B. Jiang, *Broadband moth-eye antireflection coatings on silicon.* Applied Physics Letters, 2008. **92**(6).